AEDC-TR-79-5

WING/STORE FLOW-FIELD MEASUREMENT AT TRANSONIC SPEEDS USING A LASER VELOCIMETER

F. L. Heltsley and V. A. Cline
ARO, Inc., a Sverdrup Corporation Company

PROPULSION WIND TUNNEL FACILITY
ARNOLD ENGINEERING DEVELOPMENT CENTER
AIR FORCE SYSTEMS COMMAND
ARNOLD AIR FORCE STATION, TENNESSEE 37389

April 1979

Final Report for Period April 18, 1977 — September 30, 1978

Prepared for

AIR FORCE ARMAMENT LABORATORY/DLJC
EGLIN AFB, FLORIDA 32542

This report has been reviewed by the Information Office (OI) and is releasable to the National Technical Information Service (NTIS). At NTIS, it will be available to the general public, including foreign nations.

APPROVAL STATEMENT

This report has been reviewed and approved.

ALEXANDER F. MONEY
Project Manager, Research Division
Directorate of Test Engineering

Approved for publication:

FOR THE COMMANDER

ROBERT W. CROSSLEY, Lt Colonel, USAF
Acting Director of Test Engineering
Deputy for Operations

REPORT DOCUMENTATION PAGE		READ INSTRUCTIONS BEFORE COMPLETING FORM
1 REPORT NUMBER AEDC-TR-79-5	2 GOVT ACCESSION NO.	3 RECIPIENT'S CATALOG NUMBER
4. TITLE (and Subtitle) WING/STORE FLOW-FIELD MEASUREMENT AT TRANSONIC SPEEDS USING A LASER VELOCIMETER		5. TYPE OF REPORT & PERIOD COVERED Final Report - April 18, 1977 - September 30, 1978
		6. PERFORMING ORG. REPORT NUMBER
7 AUTHOR(s) F. L. Heltsley and V. A. Cline, ARO, Inc., a Sverdrup Corporation Company		8 CONTRACT OR GRANT NUMBER(s)
9 PERFORMING ORGANIZATION NAME AND ADDRESS Arnold Engineering Development Center/DOTR Air Force Systems Command Arnold Air Force Station, Tennessee 37389		10 PROGRAM ELEMENT, PROJECT, TASK AREA & WORK UNIT NUMBERS Program Element 61102F
11 CONTROLLING OFFICE NAME AND ADDRESS Arnold Engineering Development Center/OIS Arnold Air Force Station, Tennessee 37389		12. REPORT DATE April 1979
		13. NUMBER OF PAGES 60
14. MONITORING AGENCY NAME & ADDRESS(if different from Controlling Office)		15. SECURITY CLASS. (of this report) UNCLASSIFIED
		15a. DECLASSIFICATION/DOWNGRADING SCHEDULE N/A

16. DISTRIBUTION STATEMENT (of this Report)

Approved for public release; distribution unlimited.

17 DISTRIBUTION STATEMENT (of the abstract entered in Block 20, if different from Report)

18 SUPPLEMENTARY NOTES

Available in DDC

19. KEY WORDS (Continue on reverse side if necessary and identify by block number)

wing body configurations	pressure distribution	transonic flow
external stores	laser velocimeters	MK-83
guided bombs	shadowgraphs	M-117
flow fields	wind tunnel tests	

20 ABSTRACT (Continue on reverse side if necessary and identify by block number)

A test was conducted in the AEDC Aerodynamic Wind Tunnel (1T) of the Propulsion Wind Tunnel Facility (PWT) to measure the flow fields about 5-percent models of several wing/store configurations. Test models included a wall-mounted swept wing and MK-83 and M-117 stores. Flow-field velocity measurements, made using a 2-component laser velocimeter, are presented together with model surface pressures and shadowgraphs.

DD $_{1\ JAN\ 73}^{FORM}$ 1473 EDITION OF 1 NOV 65 IS OBSOLETE

PREFACE

The work reported herein was conducted by the Arnold Engineering Development Center (AEDC), Air Force Systems Command (AFSC), at the request of the Air Force Armament Laboratory (AFATL/DLJC), AFSC. The AFATL Project Monitor was Capt. R. Grow. The results presented were obtained by ARO, Inc., AEDC Division (a Sverdrup Corporation Company), operating contractor for the AEDC, AFSC, Arnold Air Force Station, Tennessee, under ARO Projects No. P34A-D4A, P41A-P5A, and P34A-S8A. The manuscript was submitted for publication on November 17, 1978.

CONTENTS

ILLUSTRATIONS

Figure

3

TABLE

4

1.0 INTRODUCTION .

The lack of accurate experimental data has been a major restriction to the development of analytical techniques for computing wing/store flow fields. Shock waves embedded in the flow fields, often accompanied by regions of flow instability, make measurement by conventional means unreliable. Mechanical probe interference sometimes severely alters the quantities being measured. The laser velocimeter (LV) is capable of obtaining nonperturbed aerodynamic data of the type required. This investigation was conducted to obtain the velocity distributions in the transonic flow field surrounding a store within the interference flow fields of a wing and additional stores. The flow-field surveys were conducted in the Arnold Engineering Development Center (AEDC) Aerodynamic Wind Tunnel (1T) (Tunnel 1T) using a two-component LV system. Model surface pressure and shadowgraph data were also obtained for the wing/store configuration and for several single and multiple store combinations.

2.0 APPARATUS

2.1 TEST FACILITY

The AEDC Tunnel 1T is a continuous flow, open-circuit wind tunnel that can be operated over a Mach number range from 0.20 to 1.50. The tunnel operates at a constant stagnation pressure of approximately 2,850 psfa with the capability of varying the stagnation temperature from 80 to 120°F above ambient temperature. A complete description of the facility is included in Ref. 1.

The four test section walls were perforated with the exception of the window areas. A flat-ground and polished LV-quality window was installed in the sidewall adjacent to the LV from station 14.6 to station 26.6. The wing mount and a lower quality plexiglass port were located between the same tunnel stations along the opposite wall. The installation appears in Fig. 1.

2.2 TEST ARTICLES

Test hardware included two pressure instrumented 1/20-scale store models, one of the MK-83 and one of the M-117, in addition to two solid models of each store for the multiple-store configurations. The wing was swept 45 deg with a constant 6-in. chord NACA 0005-34 airfoil cross section. Dimensions of the models and the locations of the pressure orifices are presented in Figs. 2 and 3, respectively. The configuration identification and coordinate system are given in Fig. 4. The seven test configurations are shown in Fig. 5.

2.3 INSTRUMENTATION

The standard tunnel system was used to record the test conditions and model pressures. A shadowgraph system was used to determine shock locations for selected model configurations and Mach numbers. High-speed motion pictures were obtained for configuration 111 to assess its vibration characteristics and to determine the relative motion between the store and the wing. Since no significant vibration was observed, no other configurations were photographed.

A two-component LV (Refs. 2 through 7) was used to provide flow-field measurements. The LV and associated processing equipment are shown in Figs. 6 and 7, respectively.

3.0 PROCEDURE

3.1 TEST CONDITIONS

The experimental program was conducted in three phases. Phase I, involving model configurations 111, 100, and 011, was designed to investigate the mutual interference between the selected wing and a single MK-83 store at a transonic Mach number. The particular tunnel condition, $M_\infty = 0.92$, was determined experimentally as the lowest Mach number for which a shock (shown in Fig. 8) was firmly established between the store and the wing lower surface (configuration 111). Configurations 100 and 011 were tested at the same tunnel condition so that zero interference data could be recorded for both the wing and the store.

Phase II of the test program included the MK-83 single and multiple-store configurations (011, 012, and 013). The models were tested at selected Mach numbers from 0.60 to 1.30.

In Phase III, the two M-117 multiple-store configurations (022 and 023) were investigated at test conditions similar to those in Phase II.

A complete summary of test conditions is contained in Table 1.

3.2 DATA ACQUISITION

Flow-field surveys were made using the LV system previously described. Nominally, 1,000 individual particle velocities were recorded for use in the determination of the flow properties at each selected point in the flow field. In most instances two minutes were

required to complete an acquisition cycle, including the time required to reposition the traversing system. Measurements within the wake or the boundary layer usually required more time.

The focal volume position relative to the test model was recorded for each velocity data set. Periodic corrections were found to be necessary, however, to minimize spatial error caused by temperature effects. Since thermal expansion caused significant axial movement of the wind tunnel, the linear displacement transducer shown in Fig. 9 was used to monitor test section position. The output of the device was automatically combined with the traverse axial position indicator signal by the computer to provide an accurate relative measurement.

3.3 DATA REDUCTION

Analysis of the data was conducted using the digital computer software described in Ref. 2. The statistical quantities computed for each data set include mean and mode velocities, standard deviation, skewness, flatness factor (kurtosis) and Reynolds stress.

By taking advantage of the three-way symmetry of configurations 013 and 023 and assuming a resulting symmetry of the flow, it has been possible to resolve the component of velocity not measured directly by the velocimeter. As can be seen in Fig. 10a, three planes of symmetry exist, each rotated 120 deg from the others about the configuration centerline. Those sectors denoted by I are identical. Those denoted by II are also identical and are a mirror image of the adjacent sector (I).

The velocity components, V_x and V_z, were measured in constant x planes at points A through G and a through g. Exercising the symmetry as illustrated in Fig. 10b results in two vectors at each location. The measured vectors are, however, expressed in different coordinate systems. To determine the resultant velocity or the velocity component, V_y, one or both of the measured components must be transformed into the x, y, and z reference frame. An example illustrating the operation on the vector components at point A is given in Fig. 10c. Solving the Cartesian coordinate transformation equation for the y component yields

$$V_{yA} = \frac{V_{zA} \cos \theta - V_{z'a}}{\sin \theta} \tag{1}$$

where V_{zA} and $V_{z'a}$ are the measured component vectors and θ is the rotation angle. The total velocity vector magnitude can be found by combining the computed component, V_{yA}, with the measured V_{xA} and V_{zA}.

3.4 PRECISION OF MEASUREMENTS

3.4.1 Tunnel Conditions

Care was taken to allow the tunnel to stabilize before the relatively long data-recording period. The resulting variation in mean free-stream Mach number and velocity was as follows:

Parameter	$M_\infty = 0.60$	$M_\infty = 0.80$	$M_\infty = 1.10$	$M_\infty = 1.30$
ΔM_∞	± 0.001	± 0.002	± 0.003	± 0.001
ΔV_∞ (ft/sec)	± 2.0	± 2.0	± 6.0	± 5.0

The sidewalls with windows were an additional source of Mach number uncertainty. According to the Tunnel 1T calibration (Ref. 8), use of the windows can result in significant variation in Mach number along the tunnel centerline. A statistical analysis of the centerline Mach number resulted in the following values of 2σ deviation from the mean free-stream Mach number:

$M_\infty =$	0.60	0.80	1.00	1.10	1.20	1.30
ΔM	± 0.005	± 0.005	± 0.010	± 0.035	± 0.045	± 0.055

Model incidence angle uncertainty was less than ± 0.05 deg.

3.4.2 Spatial Resolution

The three-axis traverse system used in the test was capable of locating the LV probe volume within ± 0.005 in. of a desired location relative to the coordinate system origin. The uncertainty of model position relative to the origin, discussed previously in Section 3.2, was a potential source of significantly larger errors. Changes in the test section axial location as large as 0.25 in. were observed. By using the linear displacement transducer (Fig. 9), x-coordinate accuracy of ± 0.010 in. was maintained. However, the y and z components of tunnel motion were not continuously measured; therefore, it was necessary to frequently confirm those model coordinates using the laser velocimeter.

Determination of the vertical (z) position of the model upper surface was accomplished by lowering the focal volume from above the model until it touched the surface and then recording the vertical position of the traverse. The error introduced by the focal volume diameter was minimized by repeating the operation on the lower surface of the symmetrical

model and averaging the two traverse system readings. Using this procedure, the vertical position of the model centerline could be determined to within ±0.010 in. The results are not affected by tunnel flow angularity and are only slightly dependent upon model attitude for bodies of revolution parallel to the x axis.

A velocity scan was used to determine the lateral (y) position of the model. Laser velocity data were recorded at 15 to 20 points along a constant y-z line from one side of the model to the other in the region of high-velocity gradient near the model nose. The actual model centerline position could usually be determined to within ±0.030 in. from the symmetry of the velocity distribution in the y direction. The technique can be used for most models symmetrical about a constant y plane. The results are valid at any angle of attack as long as the yaw angle is small. An error in yaw caused by tunnel flow angularity or model misalignment can destroy the symmetry of the upward velocity distribution resulting in a larger y-position uncertainty. All the V_y distributions observed in the test were acceptably symmetrical.

3.4.3 Laser Velocimeter Measurements

The LV was found to provide velocity measurements which were usually repeatable within one percent. Laser velocimeter free-stream velocities were resolvable to within ±3 ft/sec corresponding to relative uncertainties of ±0.2 and ±0.4 percent of M_∞ = 1.30 and 0.60, respectively.

For each change in model configuration or tunnel condition, one or more LV measurements were made on the tunnel centerline near tunnel station 16.5 (x/D ≈ 6.0) for comparison with velocities provided by the standard tunnel system. Although the agreement was good below M_∞ = 1.0, the velocimeter readings were consistently two to five percent higher than the tunnel system values at supersonic speeds. It appears that the difference was caused by the adverse flow characteristics of the sidewall windows and was not LV related at supersonic Mach numbers. The calibration results presented in Ref. 8 indicate that tunnel centerline velocity in the region where the LV comparison data were obtained could have been as much as four percent higher than the tunnel mean velocity at M_∞ = 1.0. Verification of the LV calibration was based, therefore, upon correlation with the subsonic free-stream measurements.

A potential source of LV measurement uncertainty is the "particle lag problem" discussed in Refs. 4 through 7. A survey was made across the bow shock of configuration 022 at M_∞ = 1.30 to assess the magnitude of the error during the subject test. The results presented in Fig. 11 show that it required approximately 0.25 in. for the mean of the LV particle velocity distribution to again equal the velocity of the fluid following the relatively instantaneous

300-ft/sec fluid velocity decrease across the shock wave. Such a response indicates that the particle population within the fluid was made up of enough sufficiently small particles to provide accurate fluid velocity measurements in the flow field.

4.0 RESULTS AND DISCUSSION

4.1 WING/STORE INTERFERENCE

Model surface pressure coefficient distributions are presented in Fig. 12 for model configurations 111, 011, and 100. Chordwise distributions at three spanwise stations on the wing (configuration 100), computed using the method presented in Ref. 20, have been included for comparison. A theoretical axial distribution computed by the method presented in Refs. 16 and 17 for a single MK-83 store (configuration 011) has also been presented. The calculated distributions correlate well with the experimental results for both the wing only and store only. Dotted fairing lines have been included with the configuration 111 data since no calculated pressures were available.

Flow-field velocity measurements in the $y/D = 0$ plane are presented in Fig. 13 for the same wing/store configurations. The vectors represent the projection of the total-velocity vector in the survey plane.

Examination of Fig. 13 reveals significant differences in the flows resulting from the three configurations. The vectors obtained for the wing alone (configuration 100) show the effect of the wing leading edge which was located at $x/D = 1.43$ and $z/D \approx 1.4$ in the $y/D = 0$ plane. The flow appears to have turned upward and decelerated as it approached the wing leading-edge stagnation region, then accelerated downward to align itself with the wing lower surface. The wing-induced downwash propagated well into the flow field as evidenced by the vectors along the store centerline. The effect of the store nose stagnation region was stronger than that of the wing. The disturbance appears as a deflection and decrease in magnitude of the velocity vectors near the store nose. An additional effect of the store can be seen as an increase in vector magnitude in the expansion region at $x/D = 3.0$.

The configuration 111 flow field exhibits the combined effects of both the wing and store. The store shows a stronger influence except in the region very near the wing. The combined effect of the wing and store stagnation regions can be seen as a further decrease in velocity in the vicinity of the store nose and the wing leading edge. Velocities in the channel formed by the wing and store were larger at $x/D = 5.7$ than those induced by either the wing or the store alone. The presence of such velocities in that region is consistent with the pressure measurements presented in Fig. 12.

The magnitude of flow-field measurements made along the x axis beneath the wing (configuration 100) are presented in Fig. 14. The data represent the distribution of velocity induced at the store centerline by the wing alone.

A survey was made across the shock wave between the wing and store of configuration 111. The measurements presented in Fig. 15 indicate that the flow accelerated from the upstream condition, V_∞ = 1,045 ft/sec, to sonic velocity at x/D = 5.0 and continued to accelerate to over 1,200 ft/sec. The fluid velocity distribution shown in the figure was deduced from the data available and has been included for comparison with the LV particle velocity measurements. The distribution is based upon the shock location from the Fig. 8 shadowgraph and the velocity decrease across a shock computed using the maximum measured velocity as the upstream condition. It would seem reasonable that the difference between the measured and proposed velocity distributions was caused by the "particle lag problem." However, the calculated velocity decrease was less than half of the value obtained for the Fig. 11 shock. Yet, it required four times as far (1.0 in.) for the particle velocity to readjust to that of the fluid.

If the discrepancy is to be attributed to particle dynamics, one must assume that the particle size distribution in the population was different from that in the Fig. 11 case. A significant reduction in the percentage of small, flow-following particles would be required to produce the observed result. It seems more reasonable to assume that the LV measurements reflect an unsteadiness in the flow coupled with slight changes in wing/store shock position. The effect of shock movement was probably negligible in the Fig. 11 results because of the stable nature of the bow shock.

Figure 16 illustrates the distribution of the vertical velocity component, V_z, between the configuration 111 bodies. The data were obtained in a constant z plane (z/D = 0.874). Effects of the wing appear to be dominant over those of the store. The large gradients in both the x and y directions observed between x/D = 1.0 and 2.0 show the influence of the swept wing leading-edge and wing circulation. The upwash and downwash caused by the wing angle of attack dominate the remaining profiles.

4.2 STORE-ON-STORE INTERFERENCE

Shadowgraphs of several store configurations were taken at selected wind tunnel conditions to determine the shock position and shape at each Mach number. These are presented for configurations 011, 012, and 022 in Figs. 17, 18, and 19, respectively.

The pressure distribution on the MK-83 store is presented in Fig. 20. The symbols represent the average value at each axial station. The theoretical pressure distributions denoted by the solid lines were computed using the relaxation technique described in Refs. 16 and 17. Correlation is good for all Mach numbers except $M_\infty = 1.05$. The position of the aft normal shock at $M_\infty = 1.00$ predicted by the theory to be at $x/D = 5.8$ is confirmed by both the pressure measurements and the shadowgraph shown in Fig. 17. The transition to fully supersonic flow over the store computed to occur before $M_\infty = 1.05$ is also consistent with the shadowgraph shown in Fig. 17.

Flow-field vector projections in a constant y plane for the two-store configuration are presented in Fig. 21. An unexpected flow characteristic appears in Fig. 21b for configuration 022. The velocity between the stores decreases sharply aft of the $x/D \approx 1.2$ station and remains low even beyond the aft shoulder at $x/D \approx 2.5$. This flow pattern is quite different from that observed at the lower Mach numbers for the same store configuration (Refs. 14 and 15).

Profiles of the velocity component, V_x, in the horizontal plane of symmetry of each two-store configuration are illustrated in Fig. 22 for $M_\infty = 1.1$. These data clearly verify the presence of a disturbance between the M-117 stores. In addition, a similar effect, although not nearly as strong, can be seen between the MK-83 stores. Axial distributions of the mean velocity component, V_x, and the standard deviations of both the V_x and V_z histograms were obtained by combining the data presented in Fig. 22 with additional measurements made between $x/D = 0.9$ and 2.0. These are presented in Fig. 23 for configuration 022. The velocity, V_x', appears to have reached over 1,200 ft/sec on the centerline, $y/D = 0$, at approximately $x/D = 1.4$ before decreasing suddenly to less than 200 ft/sec at $x/D = 2.5$. The corresponding standard deviation, σx, shown in the same figure, maintained the nominal free-stream value of 40 ft/sec until the flow neared the model shoulder at $x/D \approx 1.3$. The value then increased rapidly to a maximum of 400 ft/sec at $x/D = 1.6$ followed by a gradual decrease to a minimum at $x/D \approx 2.3$ of 200 ft/sec. At that point, adjacent to the model aft shoulder, both standard deviations, σx and σz, began to increase, probably as a result of the wake region turbulence.

It is significant that no increase was observed in the V_z standard deviation between $x/D = 0$ and 2.5 while the V_x standard deviation increased an order of magnitude in that distance. Similar occurrences of velocity fluctuation in only one component have been observed in previous measurements using an LV (Refs. 2 through 7, 18, and 19). In each case, the fluctuations appear to have been in conjunction with a time-dependent flow field. Based upon the extremely large standard deviation computed for the V_x data set at $x/D = 1.6$ (i.e, $\sigma x = 400$ ft/sec), it seems reasonable to assume that the flow at that point was time dependent. The high mean velocity ($V_x \approx 1,000$ ft/sec), coupled with an unusually large flatness factor value of 3.74 for the V_x data set, suggest that an unstable shock wave might

have been present, sweeping back and forth along the centerline across the measurement point. (Flatness factor or kurtosis is the fourth moment of a statistical sample and is equal to 3.0 for a gaussian distribution, Ref. 2.)

The presence of a normal shock has already been implied by the observation of supersonic flow immediately upstream at $x/D = 1.4$. Fluctuation of the shock could explain why it could not be detected in the shadowgraph in Fig. 19.

Similar distrubances were observed for configuration 022 at both $M_\infty = 0.80$ and 1.30. A statistical analysis of the LV data at those Mach numbers revealed large standard deviations and flatness factor values at the same locations within the store flow fields. The standard deviation was found to generally increase with Mach number within the gap between the stores.

No evidence of such a disturbance appeared for configuration 012 at $M_\infty = 0.80$. Fluctuations seem to have been present at both $M_\infty = 1.10$ and 1.30, although to a much lesser degree than for configuration 022. The maximum standard deviation occurred at approximately $x/D = 4.0$.

Profiles of the vertical velocity component, V_z, along lines of constant z are shown in Fig. 24 for configuration 012. Only one quadrant was investigated because of the two planes of symmetry at $y/D = 0$ and $z/D = -0.525$.

Flow-field surveys for the three-store configurations are presented in Fig. 25. The vertical position of the lower stores, which are located on either side of the survey plane, is indicated by the dotted line. No velocity data were obtained within the outlined area since the region was hidden by the nearer store.

The velocity fluctuation observed between the stores of configurations 012 and 022 was not detected in the flow fields of either three-body configuration for the test Mach numbers of 0.60 and 0.80. The highest standard deviation observed ($\sigma x = 97$ ft/sec) was near $x/D = 2.0$ of configuration 023 in the channel formed by the upper store and one of the lower stores. For configuration 013, the standard deviation remained less than the free-stream value of 35 to 40 ft/sec at both Mach numbers.

By carefully selecting survey points and using the previously described technique for resolving the third component, V_y, a more comprehensive picture of the total flow field can be obtained. Projections of the total-velocity vectors are presented in Fig. 26 for the three-body configuration. The data illustrate the highly three-dimensional nature of the flow field.

An anomaly occurs in the center of configuration 013 where three vectors of finite rather than zero magnitude exist. The resolved value of velocity at the same point for configuration 023 was computed to be zero.

5.0 CONCLUDING REMARKS

An LV was used to provide velocity measurements in the transonic flow field of several wing and/or store combinations. The LV data are consistent with shadowgraph, model pressure measurements, and available theoretical calculations. The capability of the LV to obtain nonintrusive measurements in the region between a wing and store or multiple stores has been demonstrated. The "particle lag" effects are apparently insignificant throughout the flow field except in the region immediately downstream of each shock wave.

An unexpected unsteady flow phenomena was revealed by the LV measurements in the narrow gap between two stores. The existence of the fluctuating flow illustrates the importance of considering all the information provided by the statistical analysis of each LV data set.

A technique has been developed for resolving three-component data from two-component measurements in the limited situations where favorable symmetry conditions exist.

REFERENCES

1. *Test Facilities Handbook* (Tenth Edition). "Propulsion Wind Tunnel Facility, Vol. 4." Arnold Engineering Development Center, May 1974.

2. Altstatt, M. C. "An Experimental and Analytic Investigation of a Transonic Shock-Wave/Boundary-Layer Interaction." AEDC-TR-77-47 (ADA040023), May 1977.

3. Lo, C. F., Heltsley, F. L., and Altstatt, M. C. "A Study of Laser Velocimeter Measurements in a Transonic Flow." AIAA Paper No. 76-333, AIAA 9th Fluid and Plasma Dynamics Conference, San Diego, California, July 1976.

4. Cline, V. A. and Lo, C. F. "Application of the Dual-Scatter Laser Velocimeter in Transonic Flow Research." AGARD Meeting on Applications of Nonintrusive Instrumentation in Fluid Flow Research, France, May 1976.

5. Lo, C. F. and Heltsley, F. L. "Interpretation of Laser Velocimeter Measurements in a Transonic Flow Field." 22nd International ISA Aerospace Instrumentation Symposium, San Diego, California, May 1976.

6. Hsieh, Tsuying. "Analysis of Velocity Measurements about a Hemisphere-Cylinder Using a Laser Velocimeter." Journal of Spacecraft and Rockets, Vol. 14, No. 5, May 1977.

7. Cline, V. A. "A Laser Velocimeter for the AEDC Acoustic Research Tunnel." AEDC-TR-77-53 (ADA040903), June 1977.

8. Jackson, F. M. and Sloan, E. H. "Calibration of the AEDC-PWT 1-Foot Transonic Tunnel." AEDC-TR-68-4 (AD827912), February 1968.

9. Purvis, J. "Analytical Prediction of Flowfield over Store Configurations at Near-Critical Mach Numbers." Presented at a Short Course on Store Separation Problems at High Speeds, University of Tennessee Space Institute, Tullahoma, Tennessee, July 1978.

10. Burkhalter, J. E. and Martin, F. W. "Aerodynamic Interference of Two Axisymmetric Stores at Low Supersonic Speeds." AFATL-TR-76-116, October 1976.

11. Burkhalter, J. E. "Aerodynamic Interference for Thin Bodies in Supersonic Flow." Presented at a Short Course on Store Separation Problems at High Speeds, University of Tennessee Space Institute, Tullahoma, Tennessee, July 1978.

12. Martin, F. W., Burkhalter, J. E., and Cutchins, M. A. "Summary of Analysis of Wind Tunnel Tests of Several Store Configurations at High Subsonic and Low Supersonic Speeds." AFATL-TR-76-22, March 1976.

13. Martin, F. W., Burkhalter, J. E., Purvis, J., and Martin, B. D. "Analysis and Comparison of Several Methods for Computing Aerodynamic Compressibility and Interference Effects up to Critical Mach Numbers." AFATL-TR-77-112, September 1977.

14. Martin, F. W., Saunders, G. H., Jr., and Cutchins, M. A. "Mutual Aerodynamic Interference Effects for Multiple Bodies of Revolution and Distorted Bodies of Revolution." AFATL-TR-76-47, September 1975.

15. Martin, F. W., Saunders, G. H., and Smith, C. J. "Image System Solution for Store Aerodynamics with Interference-Part I." Journal of Aircraft, Vol. 12, No. 3, March 1975.

16. Hsieh, T. "Hemisphere-Cylinder in Transonic Flow, $M_\infty = 0.7 \sim 1.0$." AIAA Journal, Vol. 13, No. 10, October 1975.

17. South, J., Jr. and Jameson, A. "Relaxation Solutions for Inviscid Axisymmetric Transonic Flow over Blunt or Pointed Bodies." Proceedings of the AIAA Computational Fluid Dynamics Conference, Palm Springs, California, July 19-20, 1973.

18. Owen, F. K. and Johnson, D. A. "Measurement of Unsteady Vortex Flowfields." AIAA 16th Aerospace Sciences Meeting, Huntsville, Alabama, Paper No. 78-18, January 1978.

19. Owen, F. K. and Johnson, D. A. "Wake Vortex Measurements of Bodies at High Angle of Attack." AIAA 16th Aerospace Sciences Meeting, Huntsville, Alabama, Paper No. 78-23, January 1978.

20. Bailey, F. R. and Ballhaus, W. F. "Comparisons of Computed and Experimental Pressures for Transonic Flows About Isolated Wings and Wing-Fuselage Configurations." Proceedings of the Langley Research Center Conference on Aerodynamic Analyses Requiring Advanced Computers, Hampton, Virginia, NASA SP-347, Part II, March 4-6, 1975.

21. Ames Research Staff. "Equations, Tables and Charts for Compressible Flow." NACA 1135, 1953.

6% Open Area
Hole Diameter = 0.125 In.
Plate Thickness = 0.125 In.

TYPICAL PERFORATED
WALL PATTERN

Section A-A

STATION NUMBER (STA.) INDICATES INCHES
FROM NOZZLE EXIT, POSITIVE DOWNSTREAM
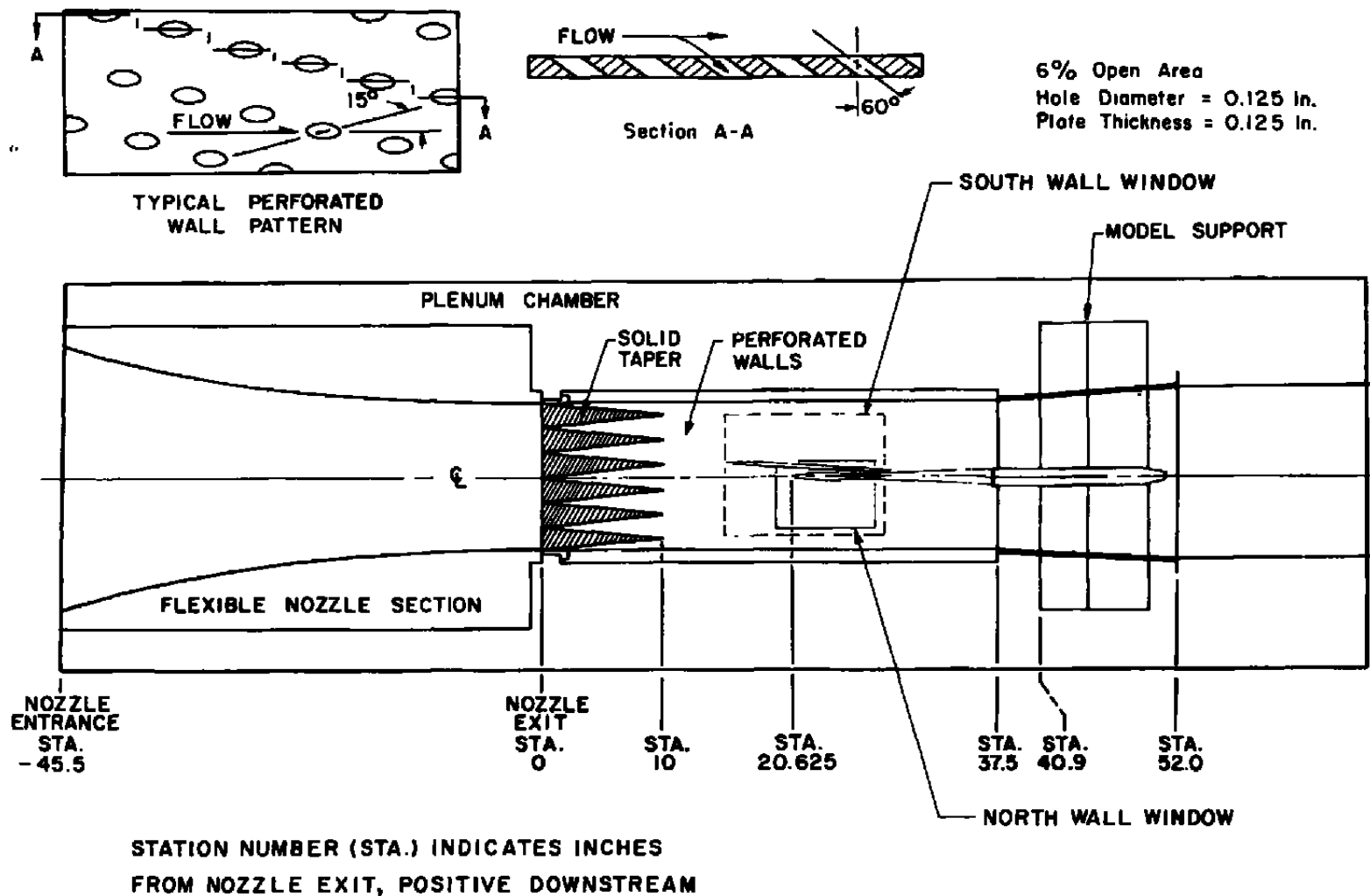
Figure 1.   Schematic of tunnel test section showing model location.

17

AEDC-TR-79-5
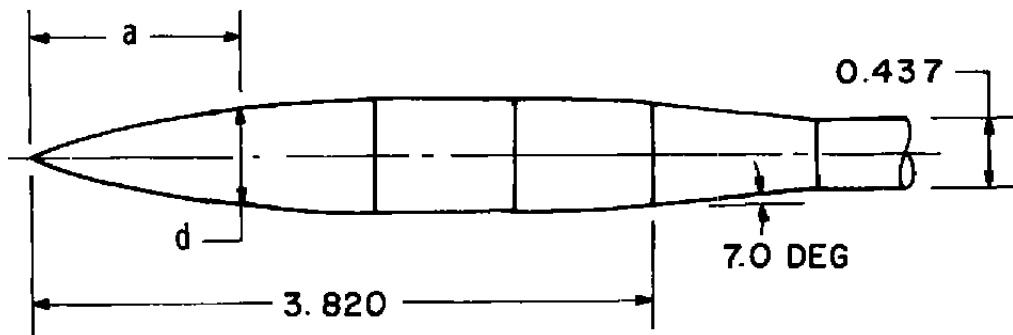
a	d	a	d	a	d
0.0000	0.0000	1.1834	0.5835	2.9833	0.7000
0.2666	0.2313	1.3167	0.6093	3.1166	0.6983
0.3834	0.3073	1.4500	0.6326	3.2500	0.6934
0.5167	0.3777	1.5833	0.6534	3.3833	0.6855
0.6500	0.4349	1.7166	0.6715	3.5166	0.6745
0.7834	0.4819	1.8500	0.6862	3.6500	0.6608
0.9167	0.5211	1.9833	0.6961	3.7833	0.6403
1.0500	0.5545	2.1166	0.7000	3.8200	0.6392

a. MK-83

ALL DIMENSIONS IN INCHES
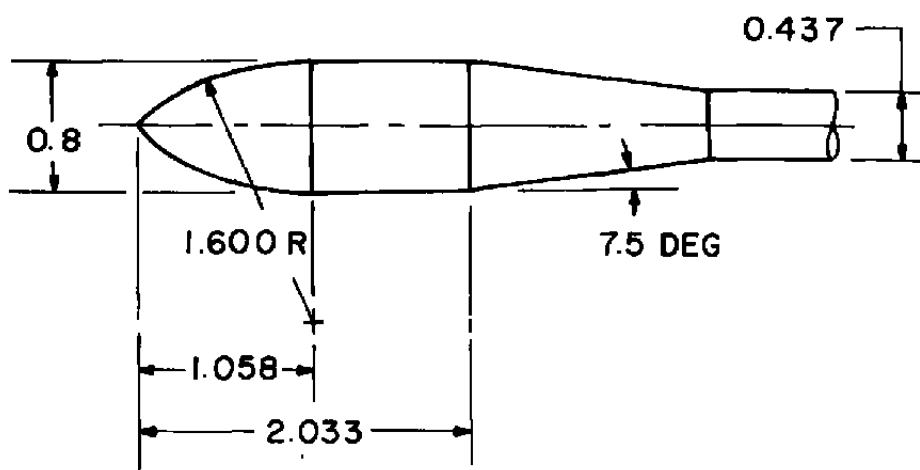
b. M-117

Figure 2. Model dimensions.

18

WIND TUNNEL SIDEWALL

6.0

8.25

45 DEG

A   A

STORE CENTERLINE
(REFERENCE)

ALL DIMENSIONS IN INCHES

x_W

t

SECTION A-A
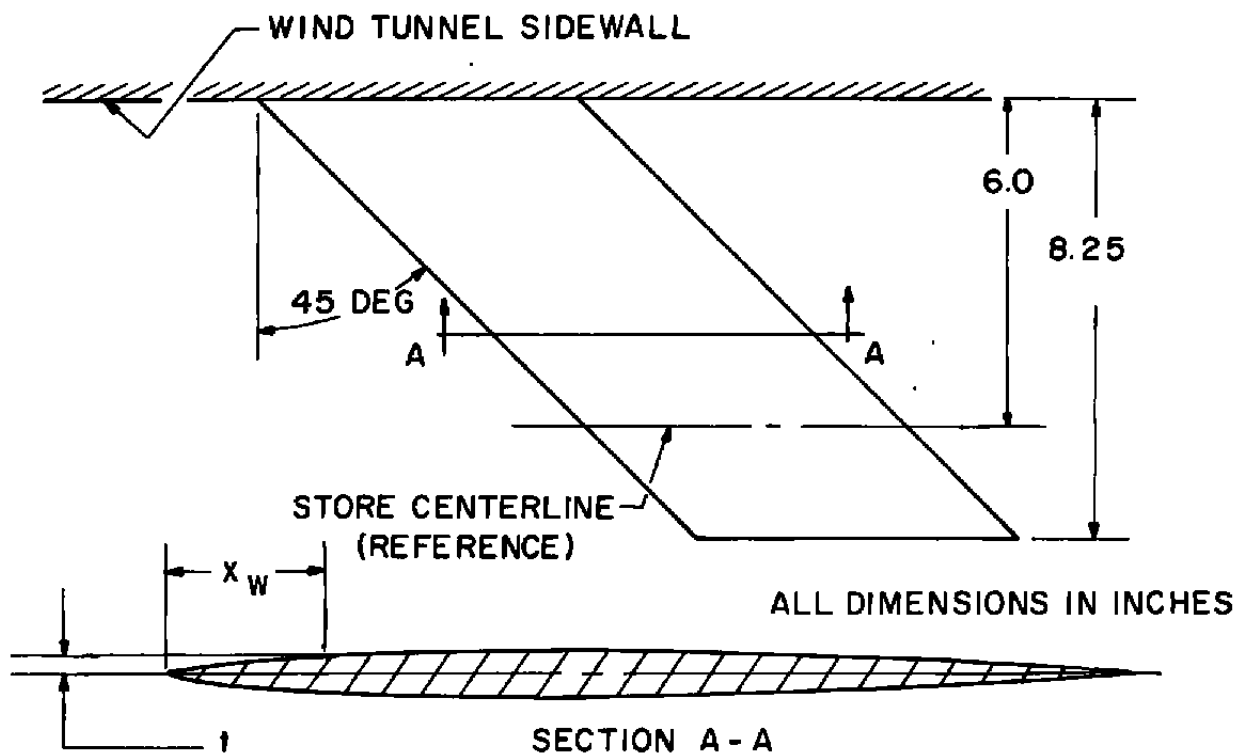
x_W	t
0.0000	0.0000
0.0065	0.0095
0.0750	0.0284
0.1500	0.0420
0.3000	0.0623
0.4500	0.0783
0.6000	0.0914
0.9000	0.1124
1.2000	0.1274

x_W	t
1.8000	0.1450
2.4000	0.1500
3.0000	0.1456
3.6000	0.1330
4.2000	0.1120
4.8000	0.0830
5.4000	0.0466
5.7000	0.0256
6.0000	0.0000

c. Wing
Figure 2. Concluded.

ALL DIMENSIONS IN INCHES

PRESSURE ORIFICES AT ϕ = 0, 90, 180, 270 DEG
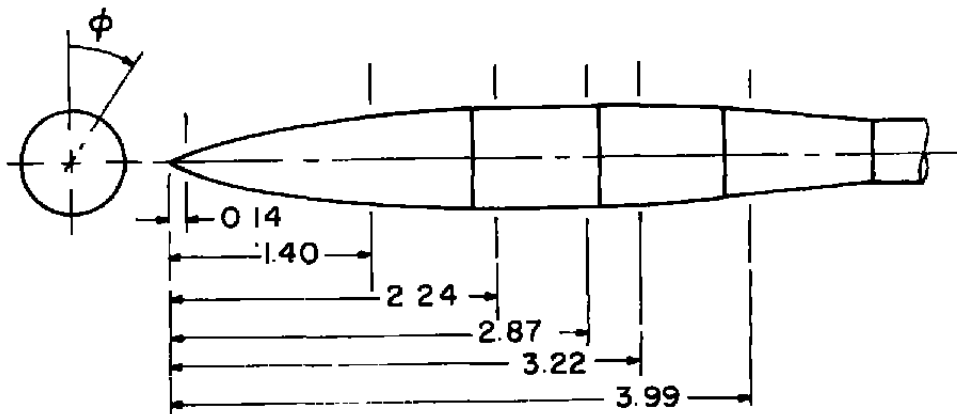
a. MK-83
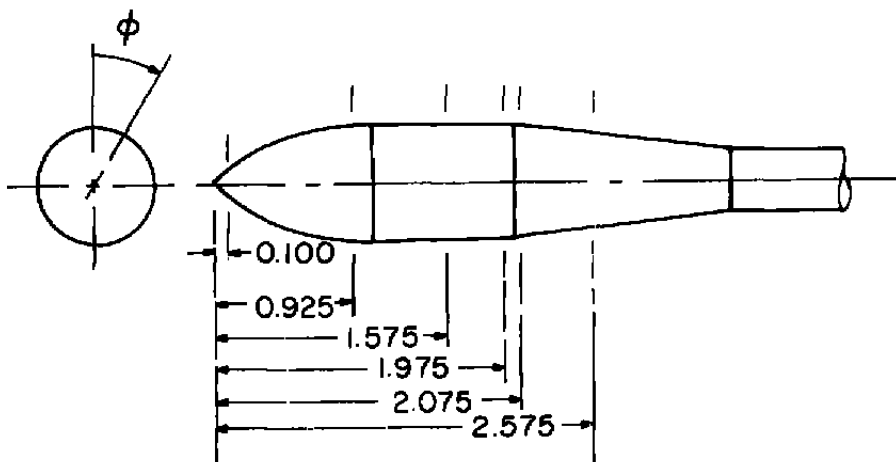
b. M-117

Figure 3. Pressure orifice locations.

ALL DIMENSIONS IN INCHES

0.15
0.90
1.80
2.40
3.60

SECTION A - A

STORE CENTERLINE

LOWER SURFACE

A

A

6.70

6.00

5.30

WIND TUNNEL
WALL
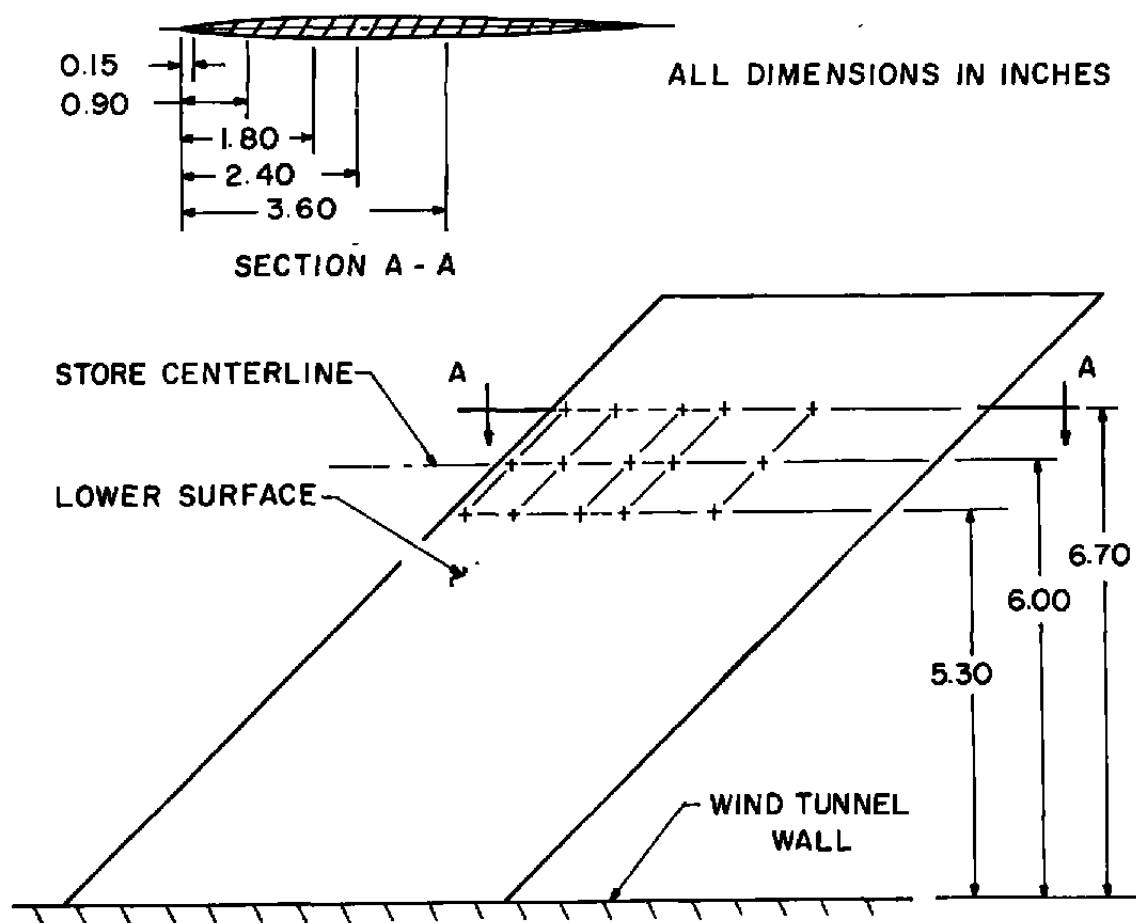
c. Wing
Figure 3. Concluded.

CONFIG ⌐W│S│N⌐

└── NUMBER OF STORES

└── STORE

S = 0 NO STORE

= 1 MK-83 (FIG. 2a)

= 2 M-117 (FIG. 2b)

└── WING

W = 0 NO WING

= 1 45-DEG SWEPT WING
8.25-IN. SPAN, 6.0-IN. CHORD
NACA 0005-34 SECTION
(FIG. 2c)
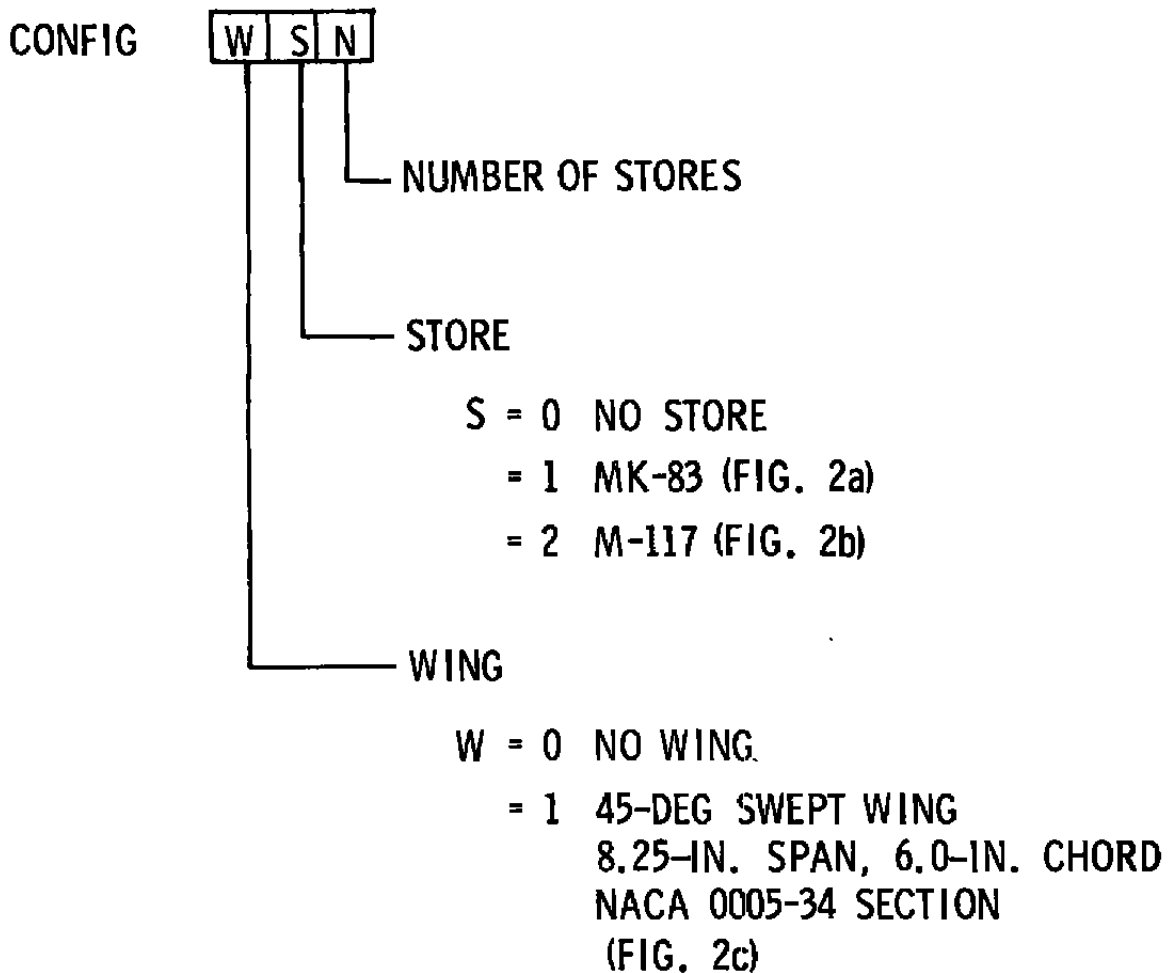
a. Configuration identification

Figure 4. Configuration identification and coordinate
system definition.

STA.
20.625
PLAN VIEW

SIDE VIEW
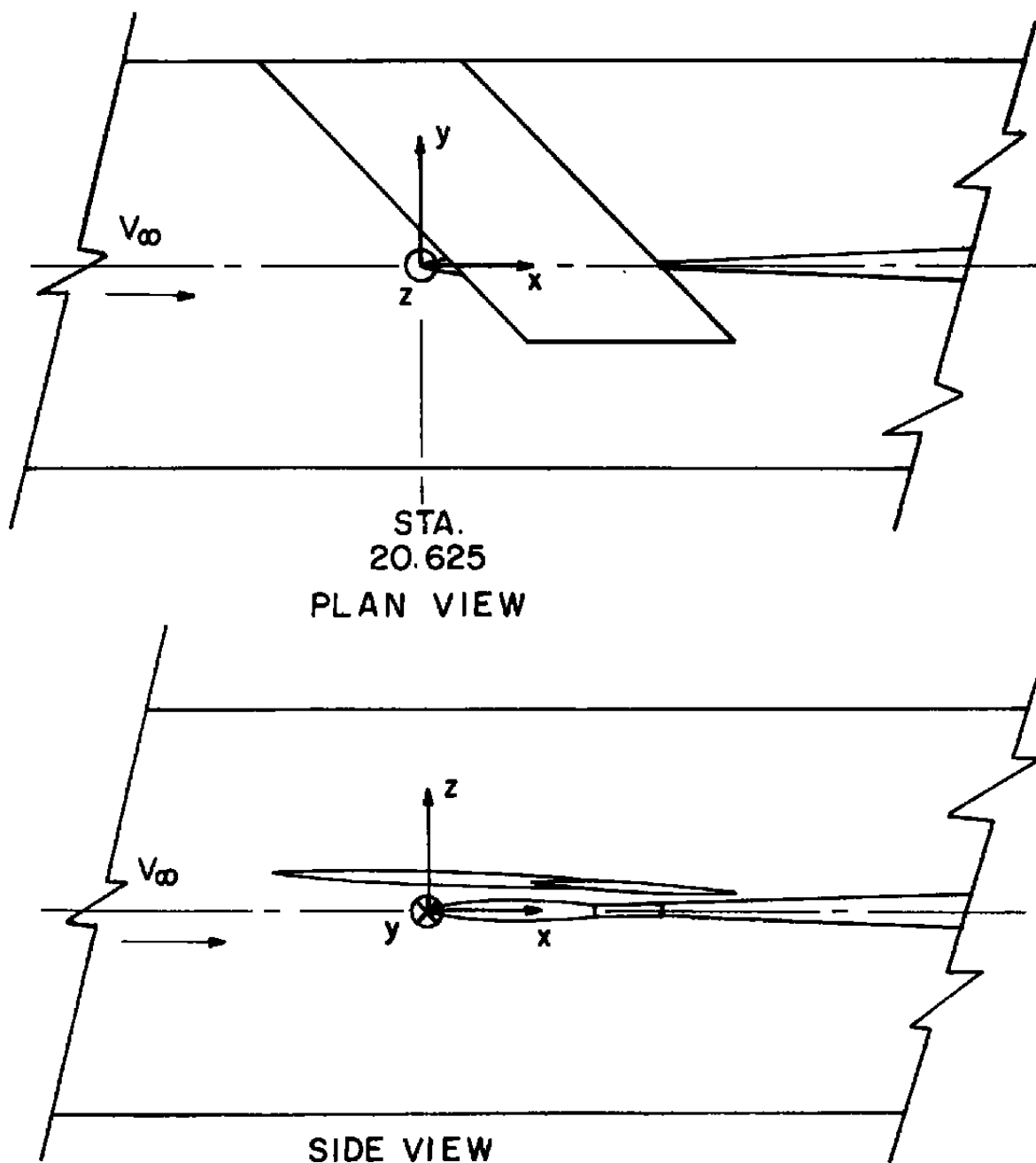
b. Coordinate system definition
Figure 4. Concluded.

23
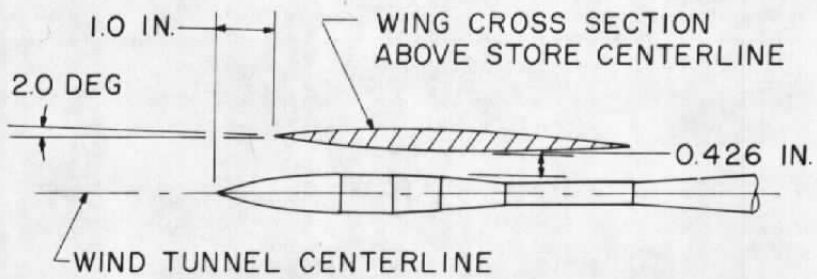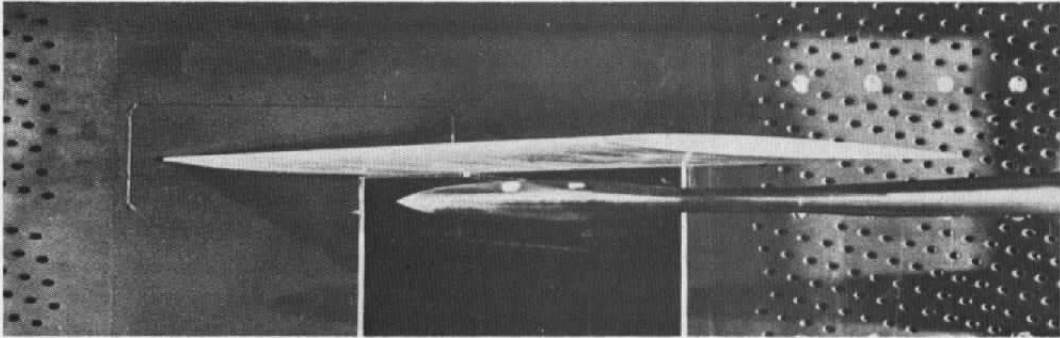
a. Configuration 111
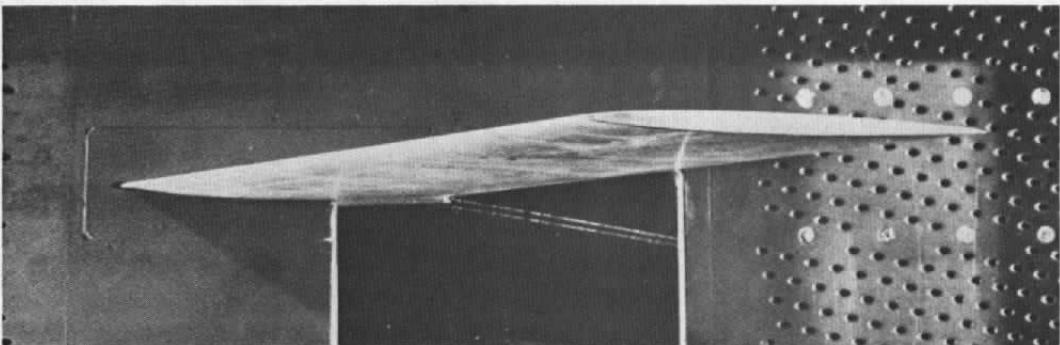
b. Configuration 100
Figure 5. Relative location of wing and stores for each
configuration.

24

● — AXIAL ROW OF PRESSURE ORIFICES
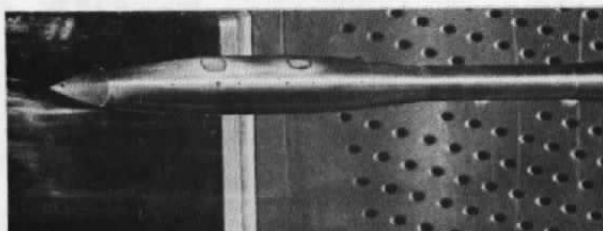
c. Configuration 011
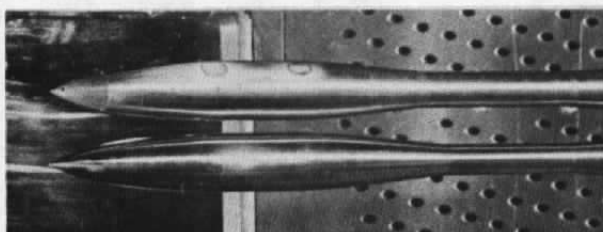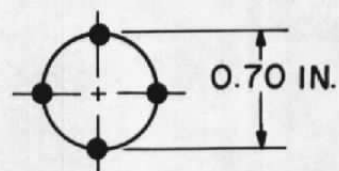
d. Configuration 012
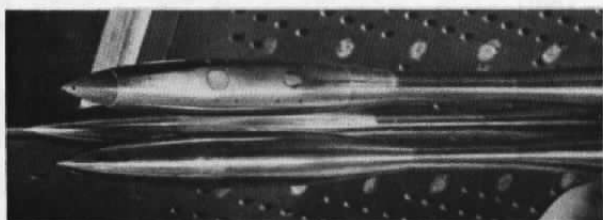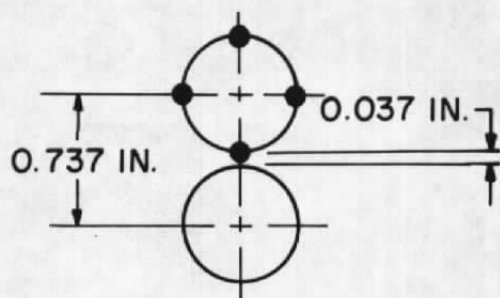
e. Configuration 013
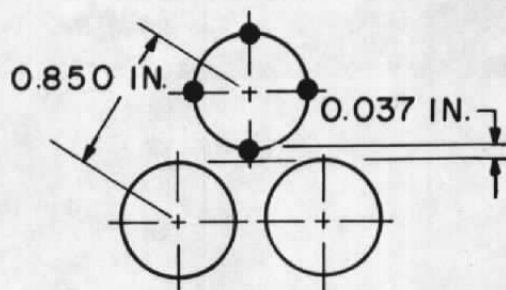
Figure 5. Continued.

● — AXIAL ROW OF PRESSURE ORIFICES
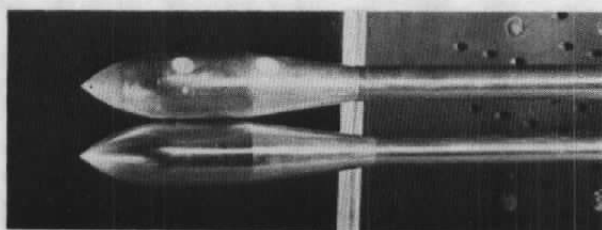
f. Configuration 022
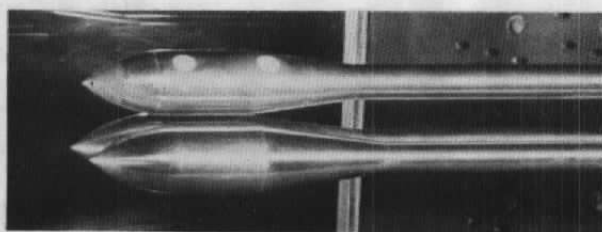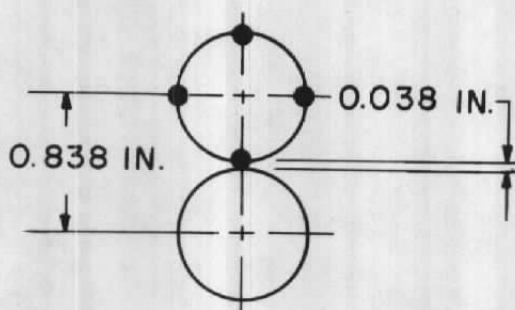
g. Configuration 023
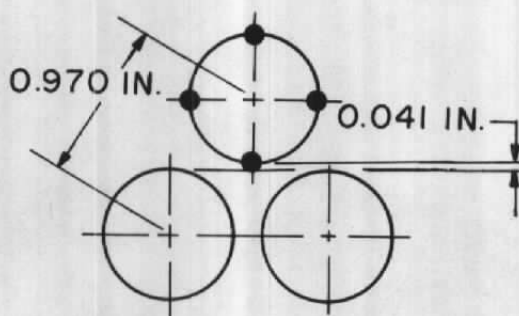
Figure 5. Concluded.

26
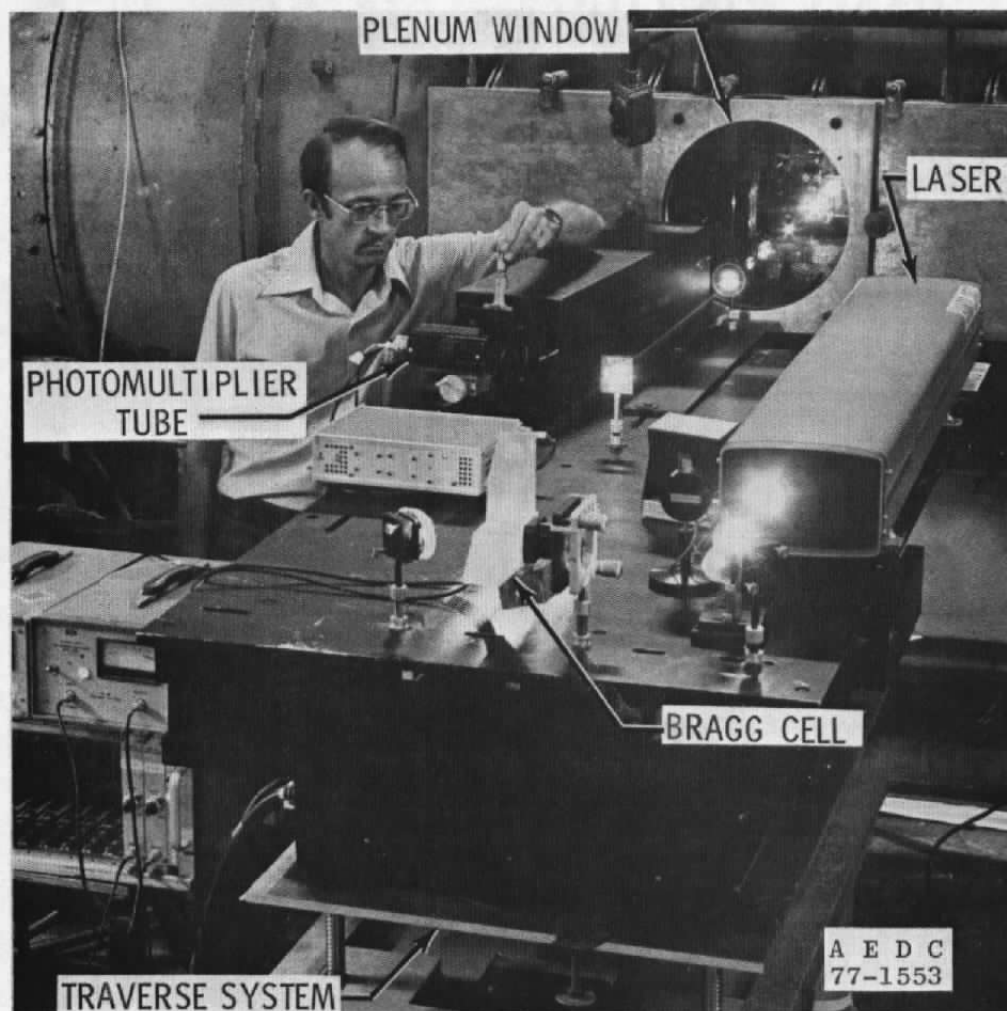
Figure 6. Laser velocimeter positioned for flow measurement in aerodynamic wind tunnel (1T).
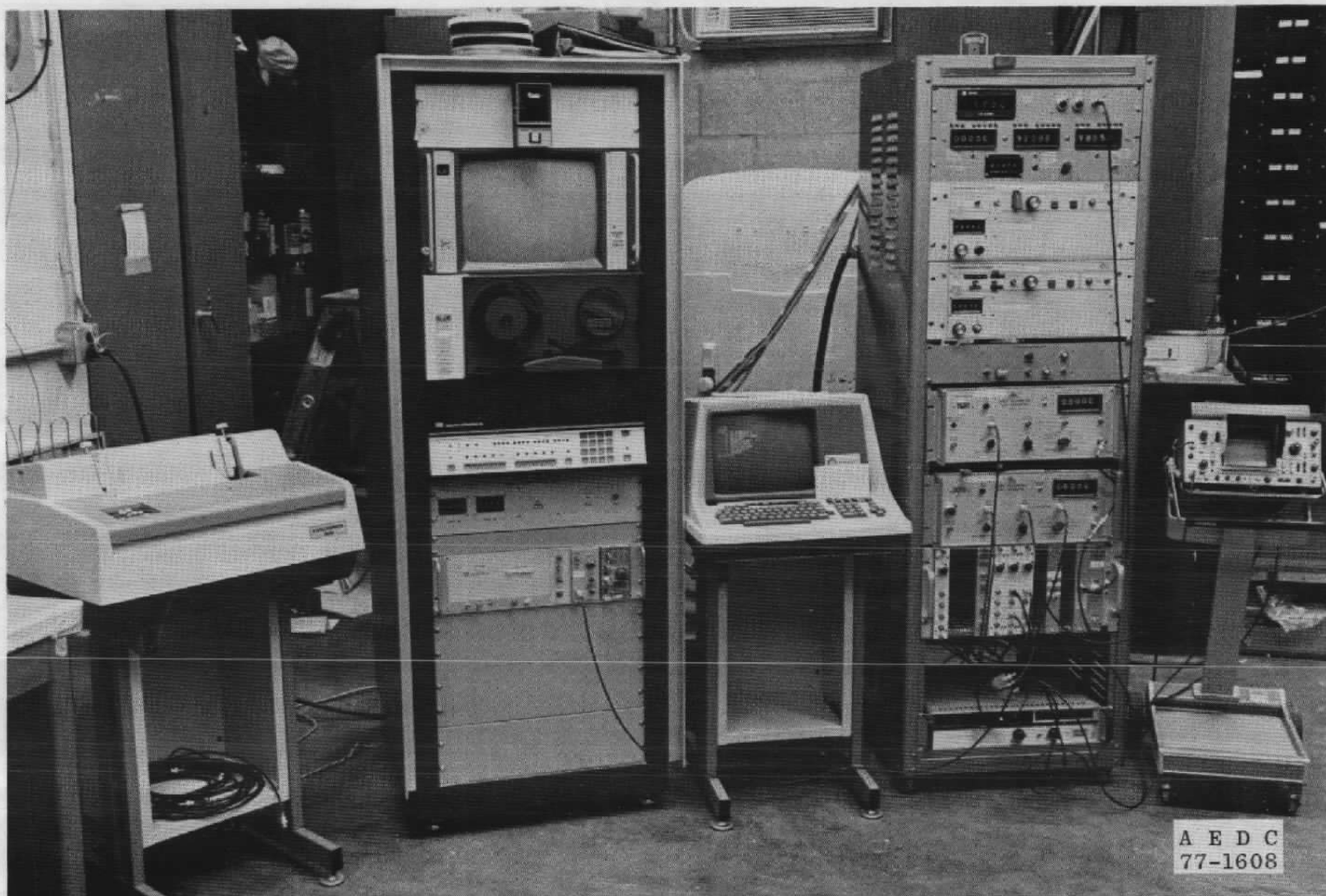
Figure 7. Laser velocimeter remote electronic processing system.
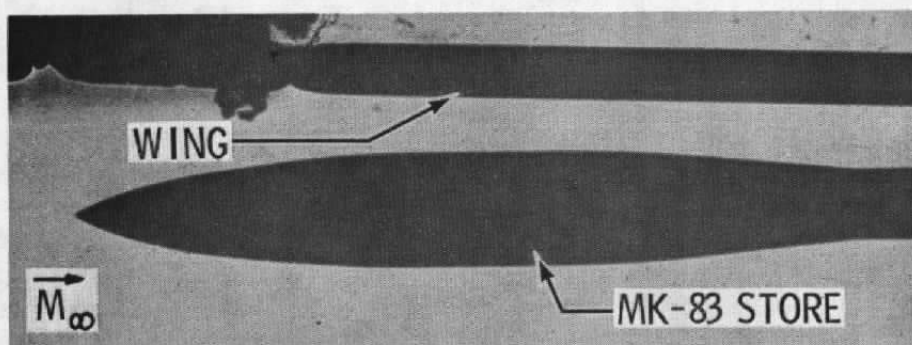
a. Wind off
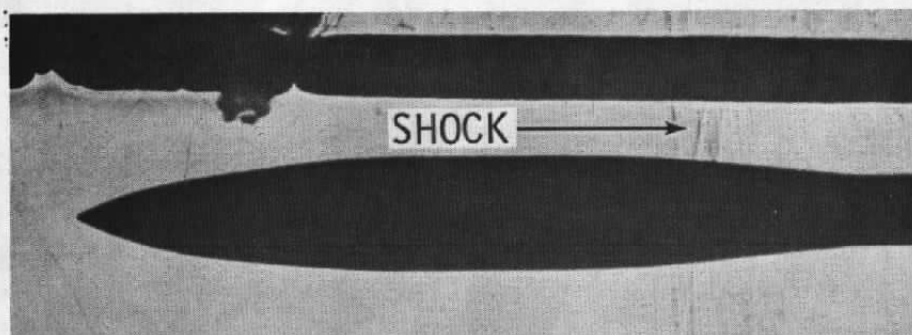
b. $M_\infty = 0.92$
Figure 8. Shadowgraphs showing shock between wing and store.
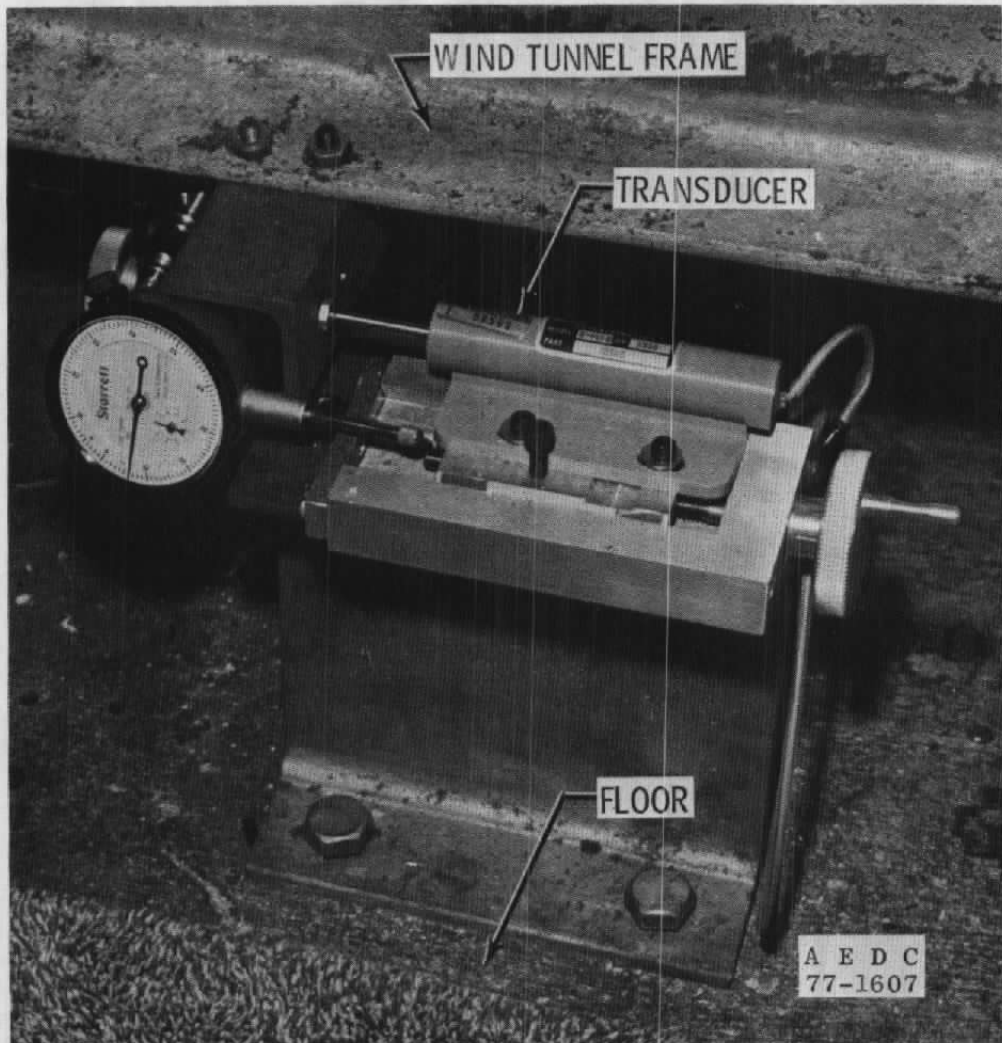
Figure 9. Device for monitoring axial movement of wind
tunnel test section.
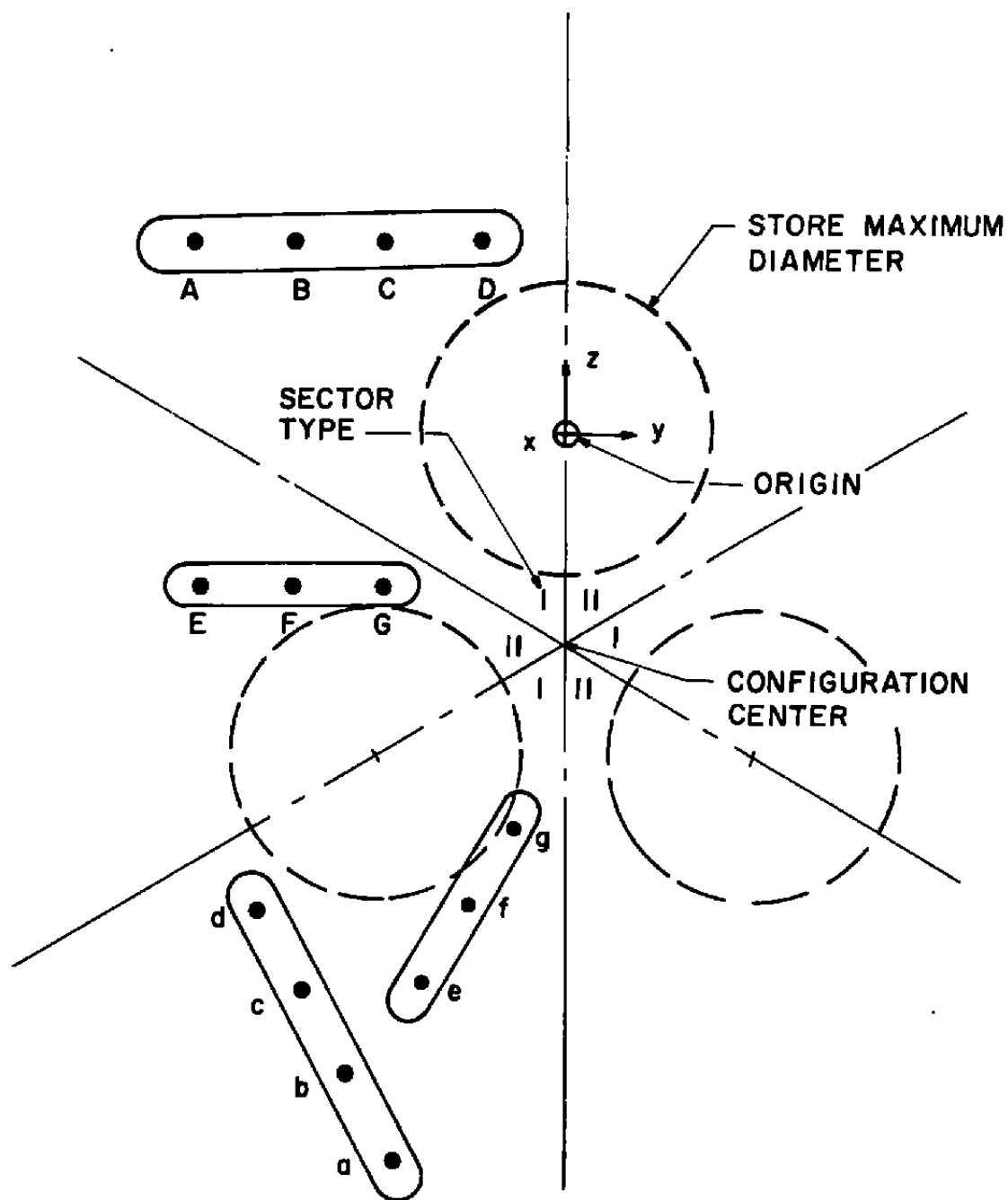
a. Survey plane measurements
Figure 10. Determination of third velocity component, V_y, from two-component measurements.

31
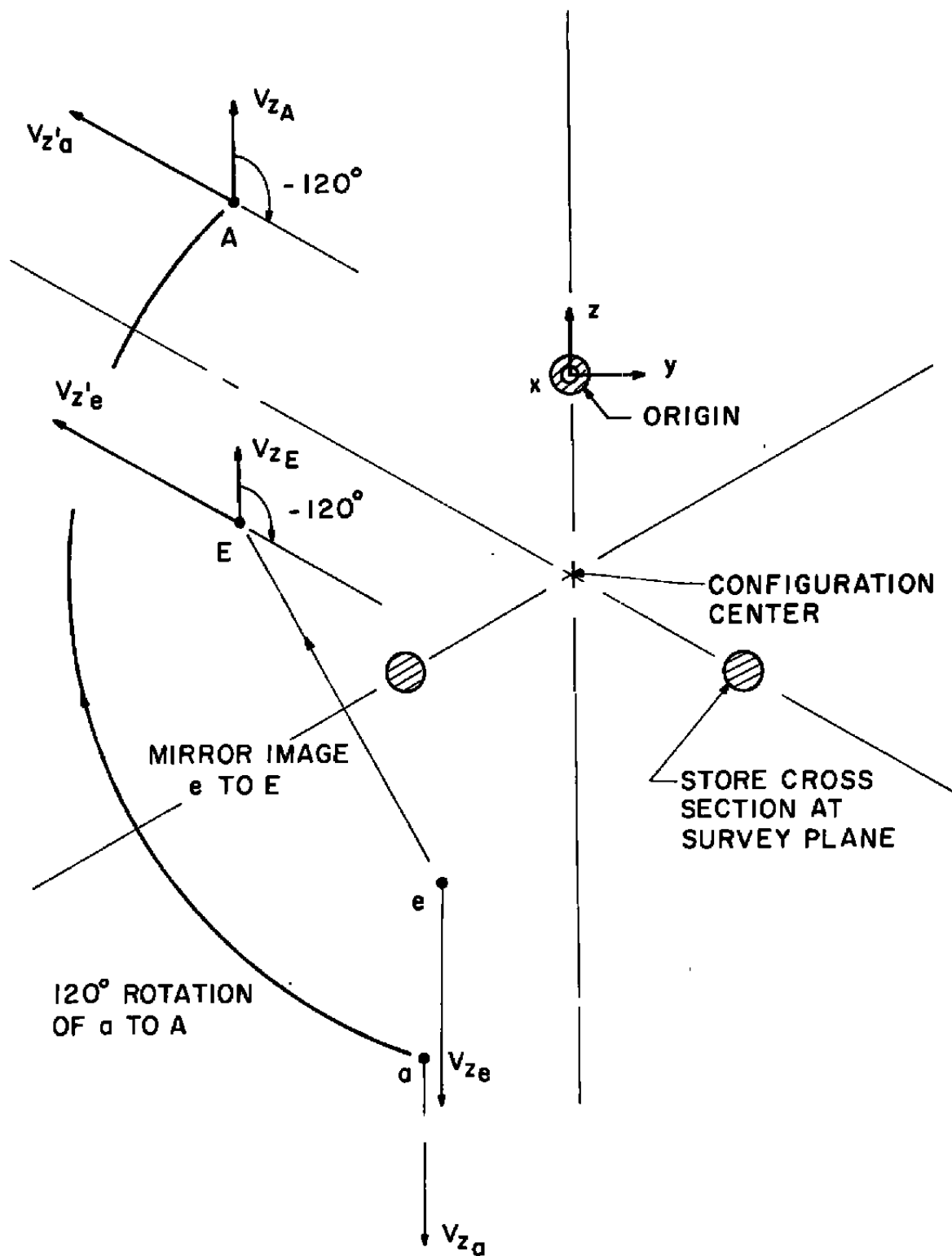
b. Symmetry assumptions
Figure 10. Continued.
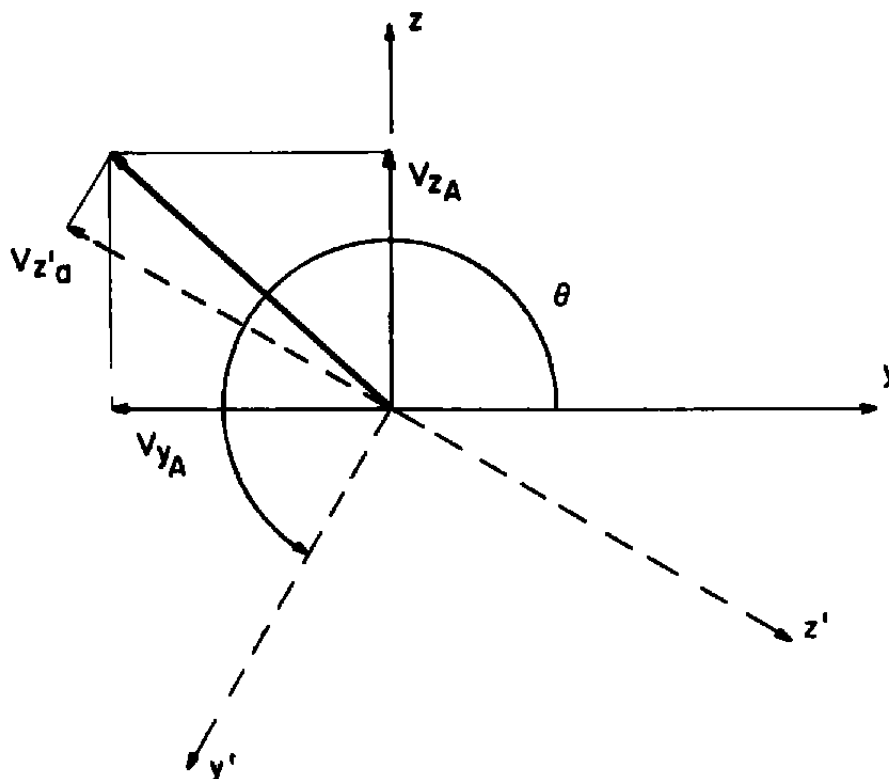
MEASURED: V_{z_A} = 80.0 ft/sec V_{x_A} = 884.0 ft/sec

$V_{z'_A}$ = - 112.0 ft/sec

FROM SYMMETRY: θ = 240° OR -120°

COMPUTED: V_{y_A} = -83.1 ft/sec   (EQ 1)

c. Velocity determination
Figure 10. Concluded.
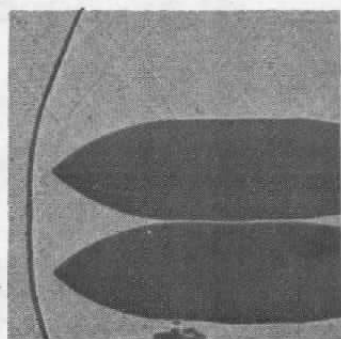
SHADOWGRAPH
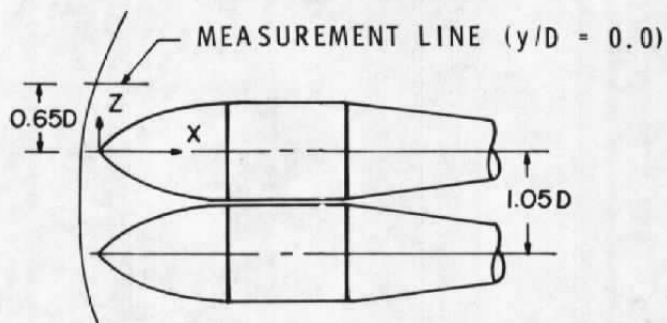
SCHEMATIC
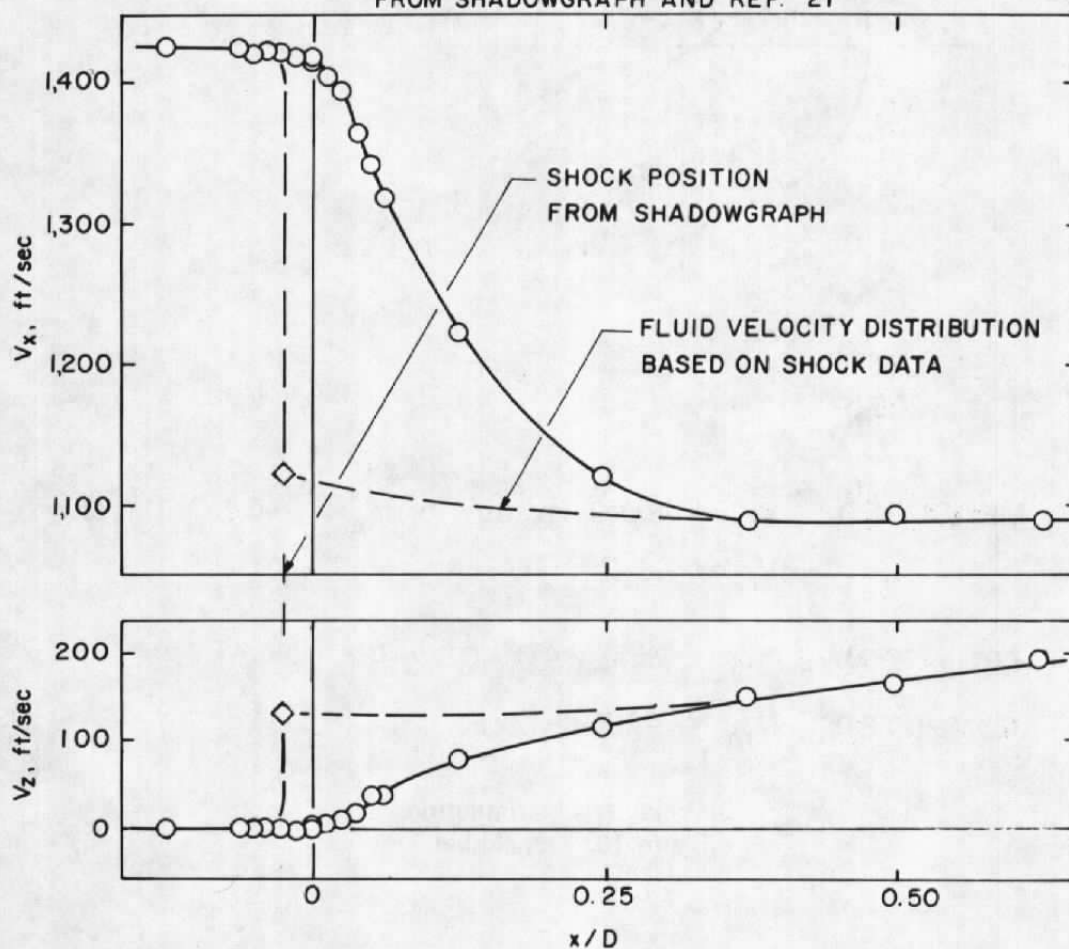
Figure 11. Velocity survey across bow shock of configuration
022, M_∞ = 1.30.

34
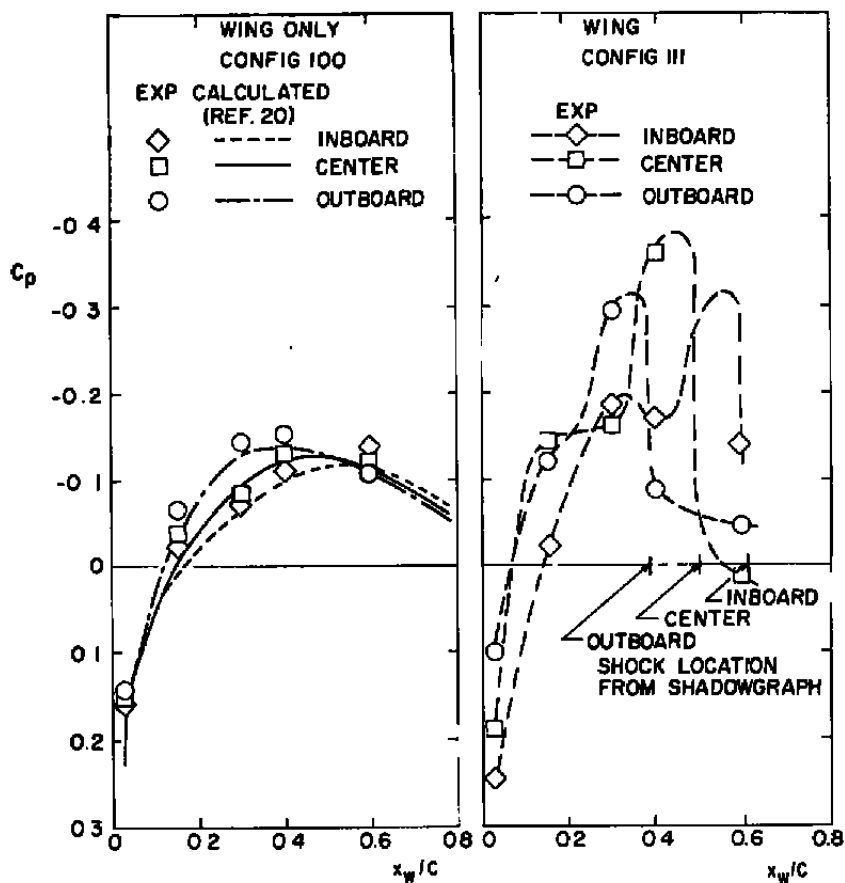
a. Wing pressure distribution
Figure 12. Interference effects of wing and store on surface
pressure coefficient, $M_\infty = 0.92$.
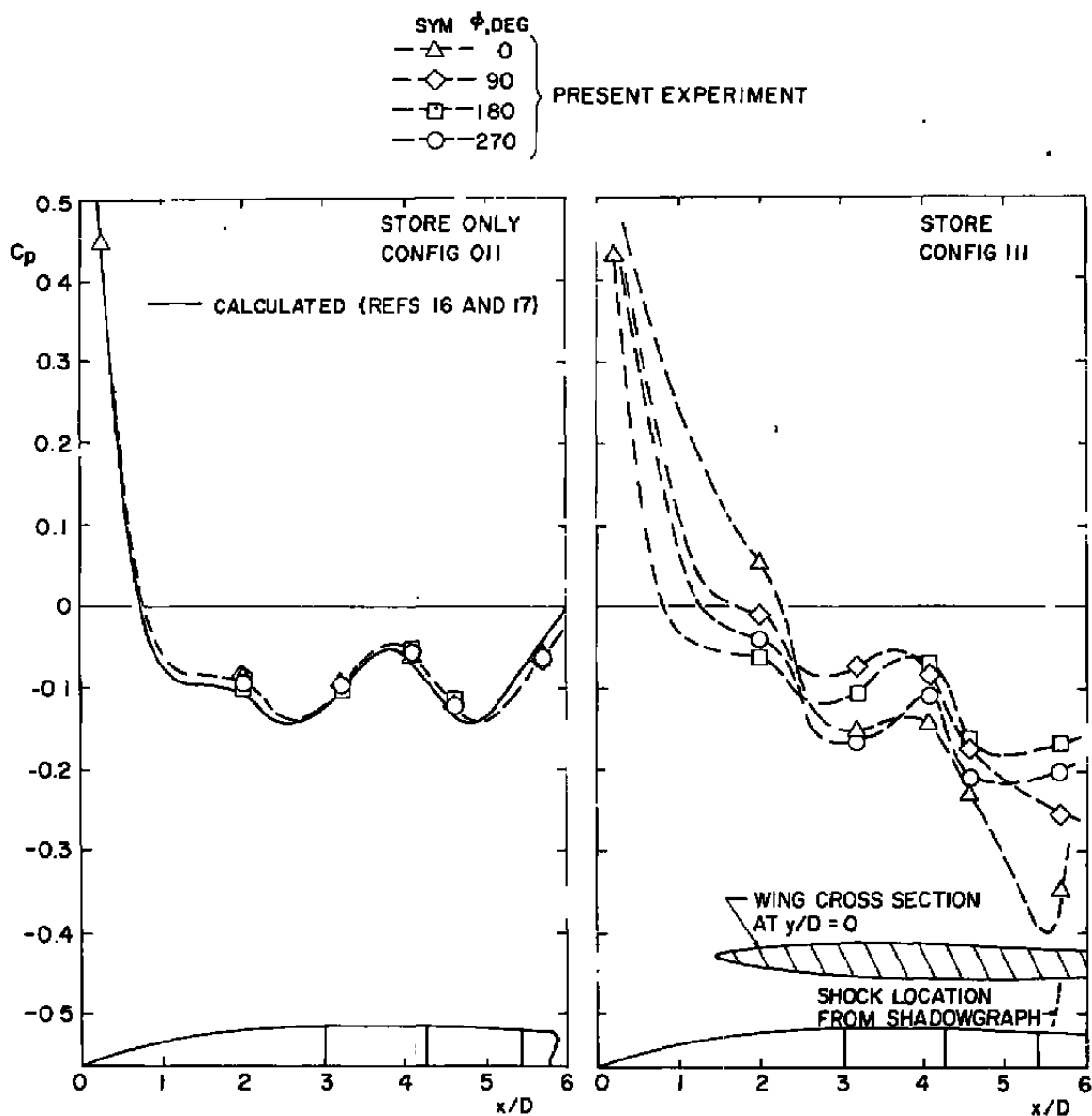
b. Store pressure distribution
Figure 12. Concluded.

z

y

x

MEASUREMENT PLANE

ORIGIN

$V_\infty = 1,045$ ft/sec

CONFIG
——— · III WING AND STORE
········· 100 WING ONLY
——— ·· 011 STORE ONLY

VELOCITY SCALE
ft/sec
0   1,000

z/D

1

0

-1

0   2   4   6

x/D
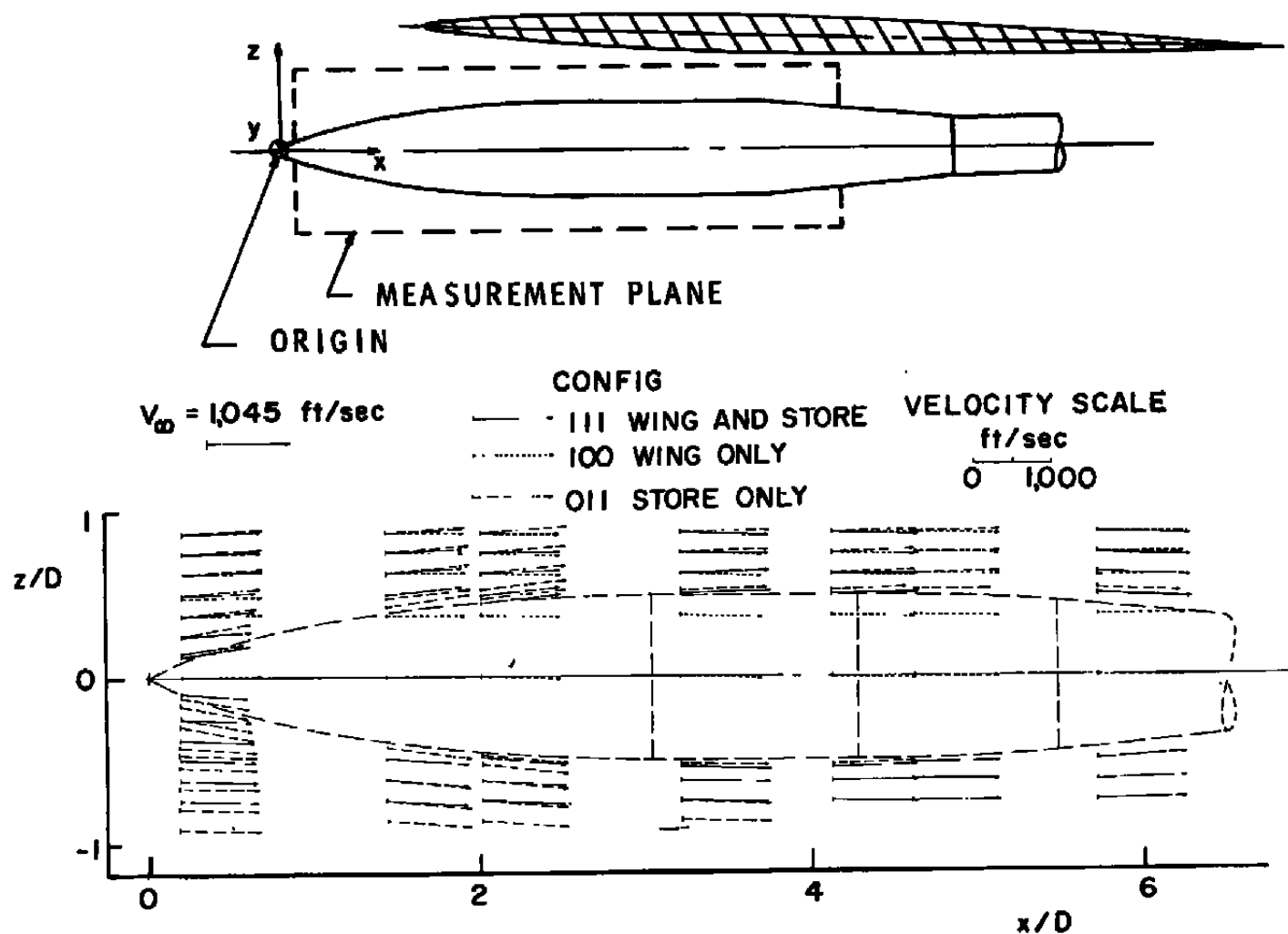
Figure 13. Flow-field survey for single-store configurations,
y/D = 0; M_∞ = 0.92.

MEASUREMENT LINE
(y/D = 0.0, z/D = 0.0)

ORIGIN

FREE-STREAM VELOCITY
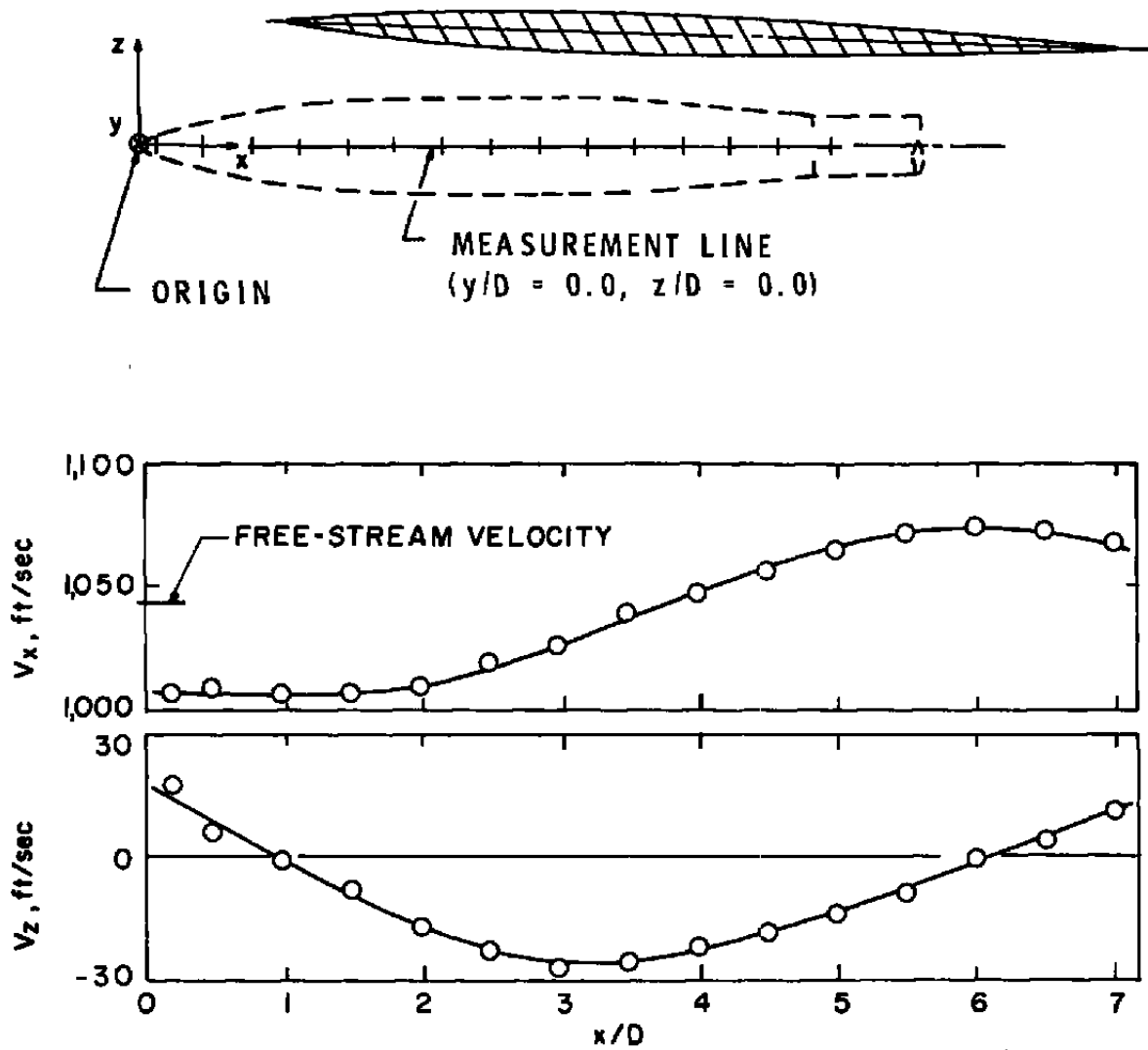
Figure 14. Survey along x axis with store removed, M_∞ = 0.92.
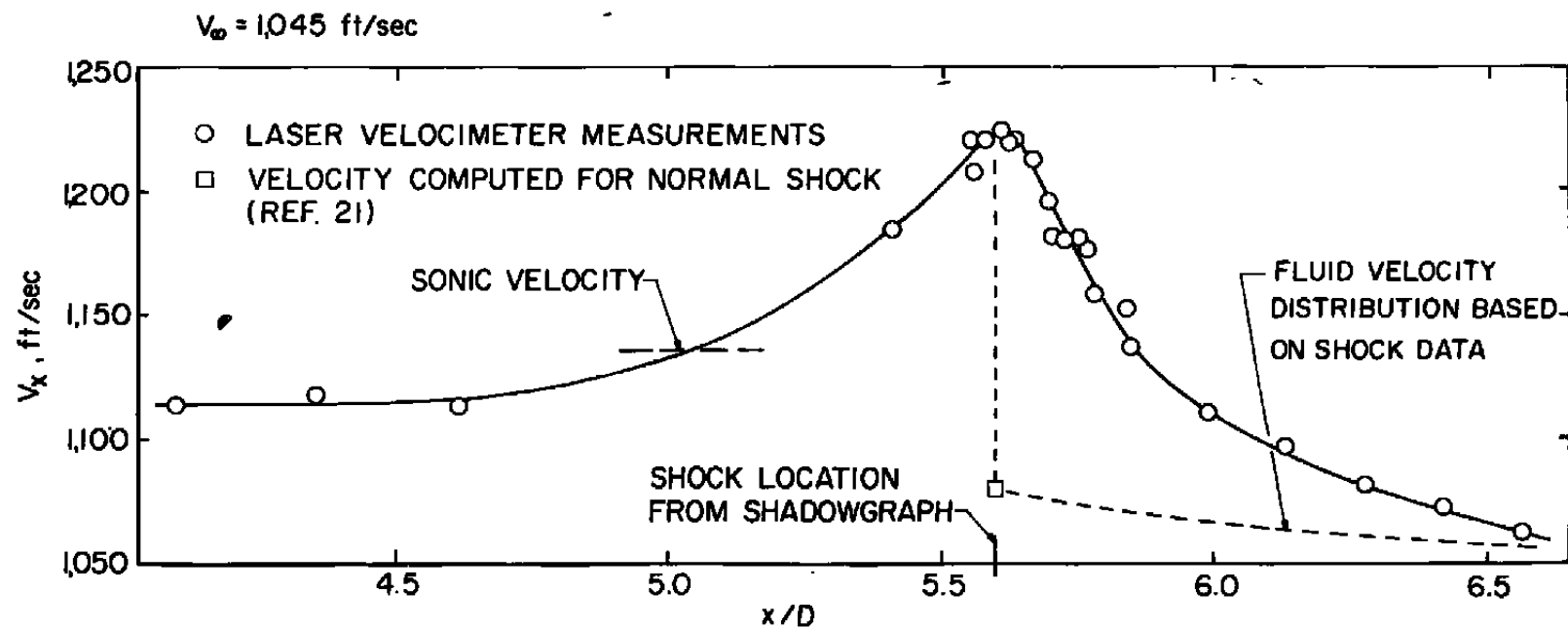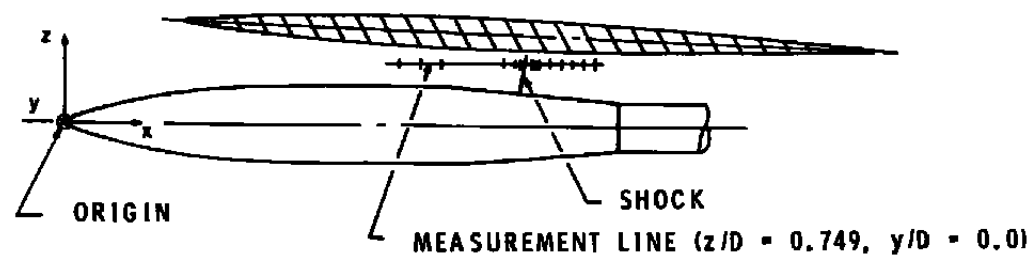
Figure 15. Flow survey across wing/MK-83 store shock, y/D = 0,
M_∞ = 0.92.
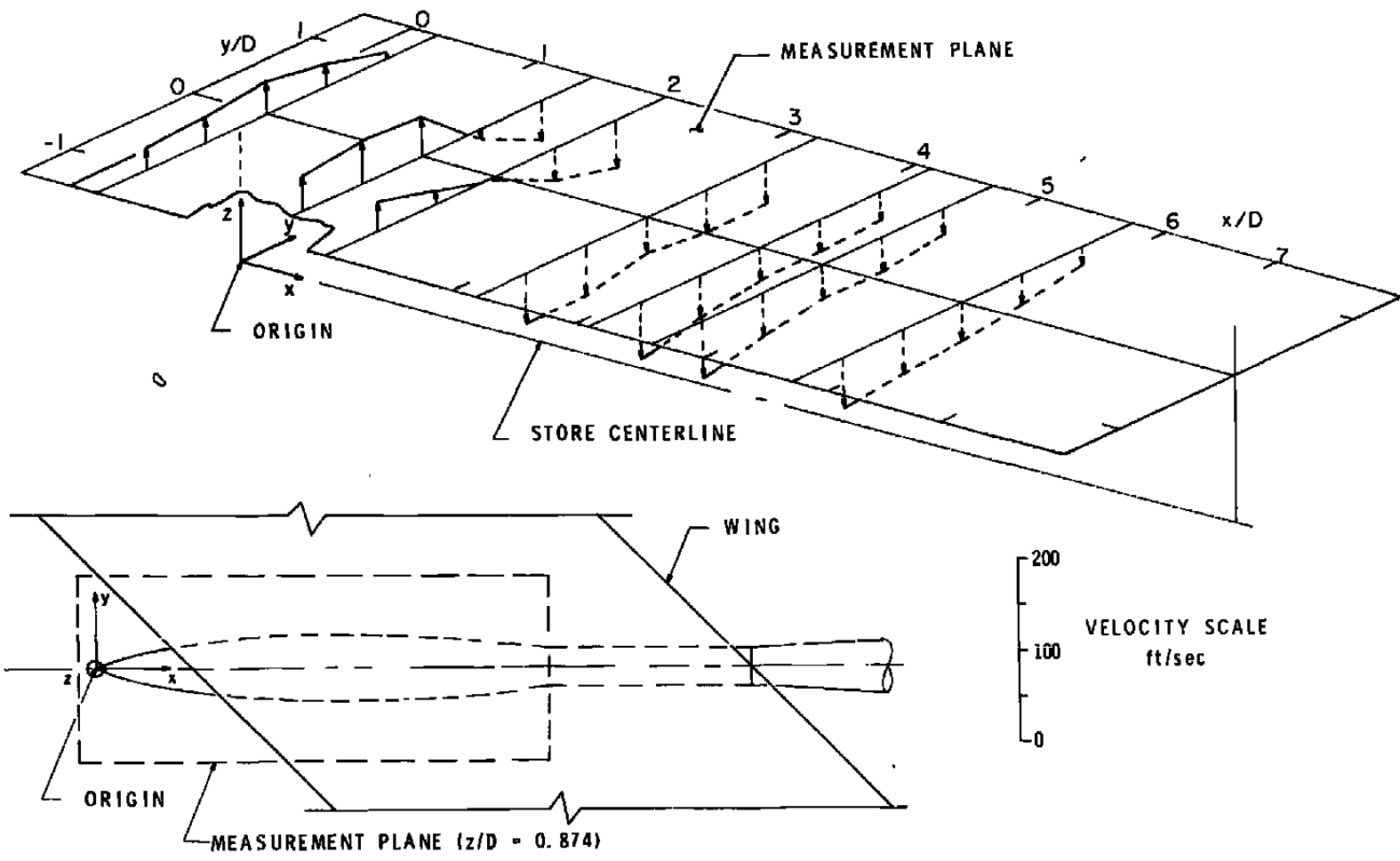
Figure 16. V_z distribution between wing and MK-83 store
(configuration 111), $M_\infty = 0.92$.
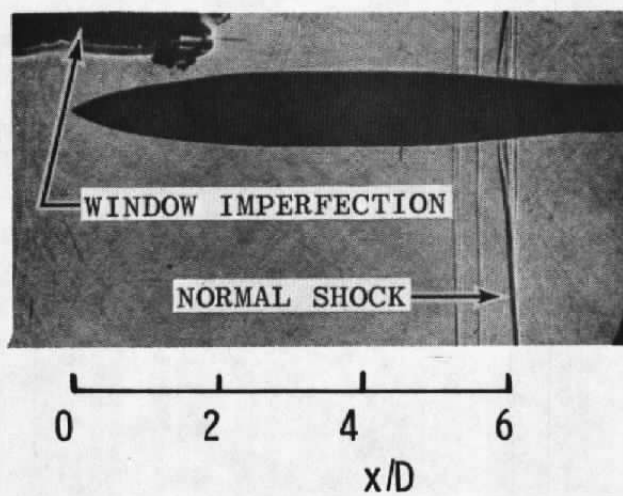
a. $M_\infty = 1.00$
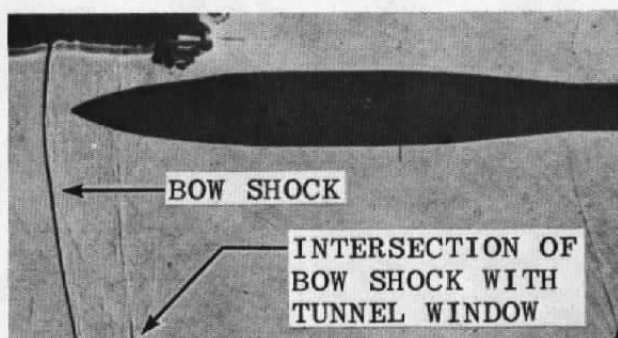
b. $M_\infty = 1.05$
Figure 17. Shadowgraphs of single MK-83 store (configuration 011).

41
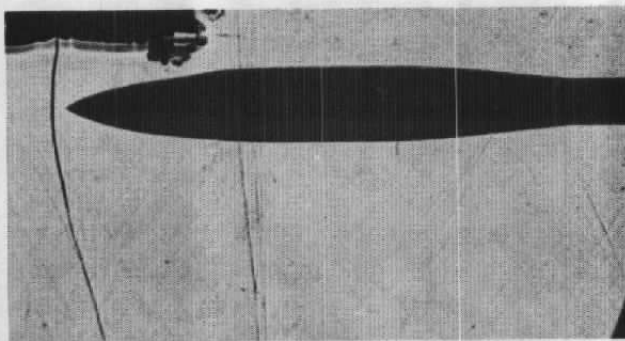
c. M_∞ = 1.10
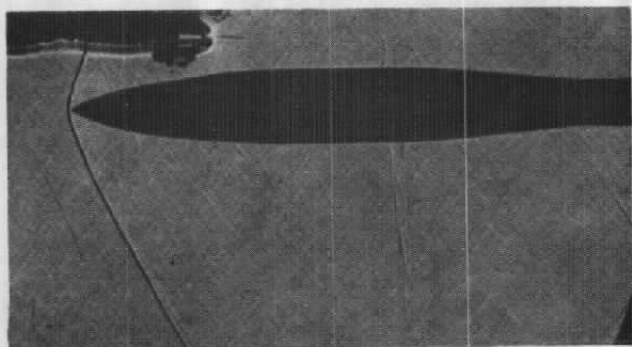
d. M_∞ = 1.20
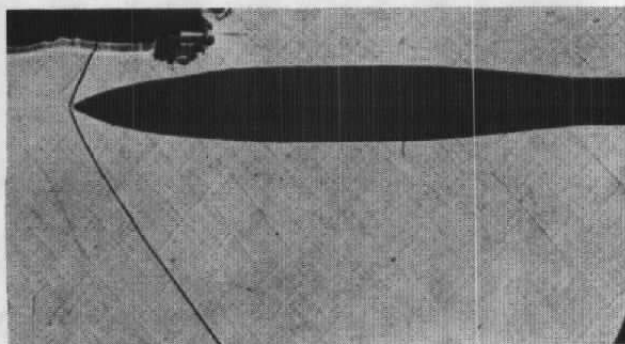
e. M_∞ = 1.30
Figure 17. Concluded.
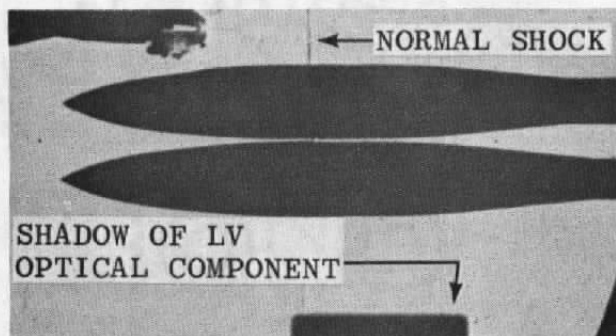
a. $M_\infty = 0.92$
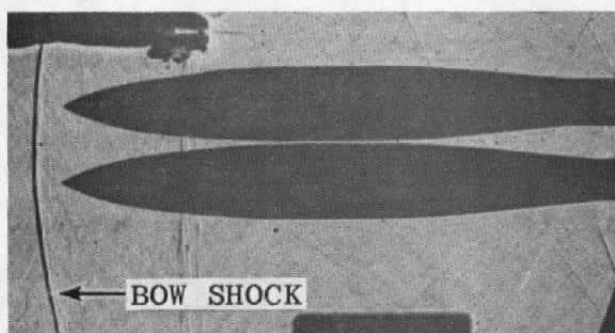
b. $M_\infty = 1.10$
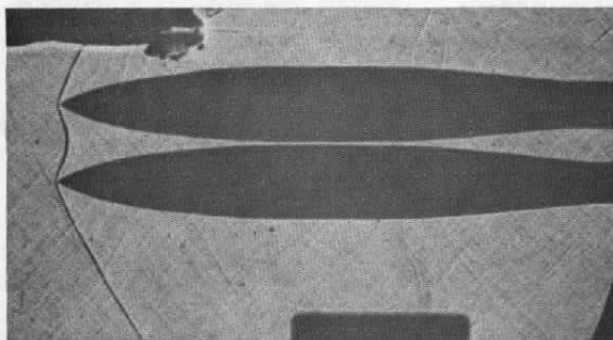
c. $M_\infty = 1.30$
Figure 18. Shadowgraphs of two MK-83 stores (configuration 012).

43
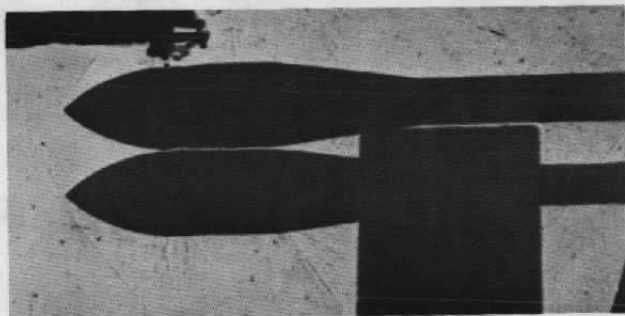
a. $M_\infty = 0.80$
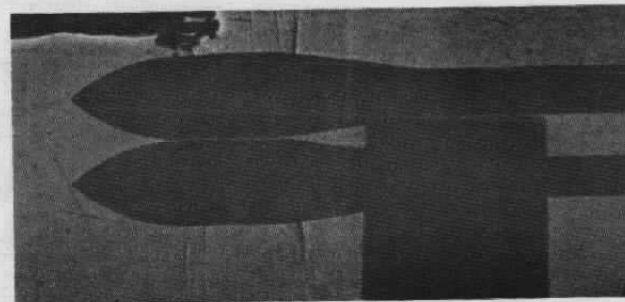
b. $M_\infty = 0.85$
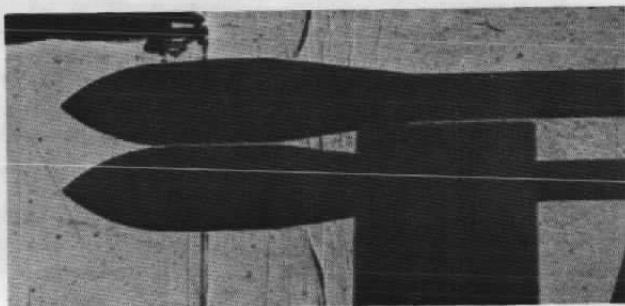
c. $M_\infty = 0.90$
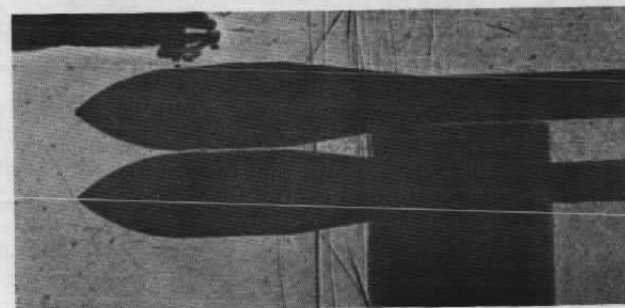
d. $M_\infty = 0.95$

Figure 19. Shadowgraphs of two M-117 stores (configuration 022).

e. $M_\infty = 1.00$

BOW SHOCK
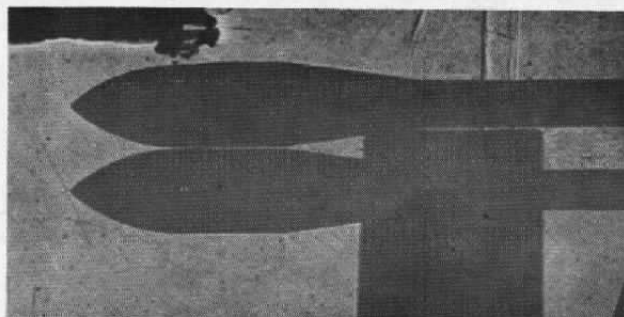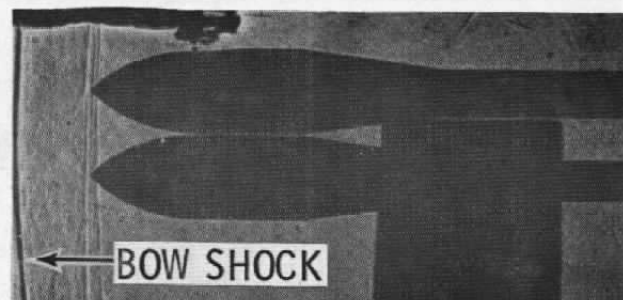
f. $M_\infty = 1.10$
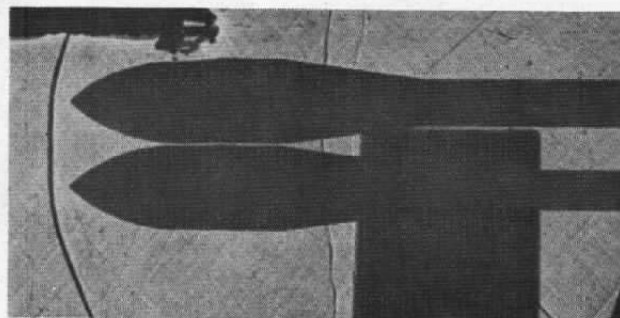
g. $M_\infty = 1.30$
Figure 19. Concluded.
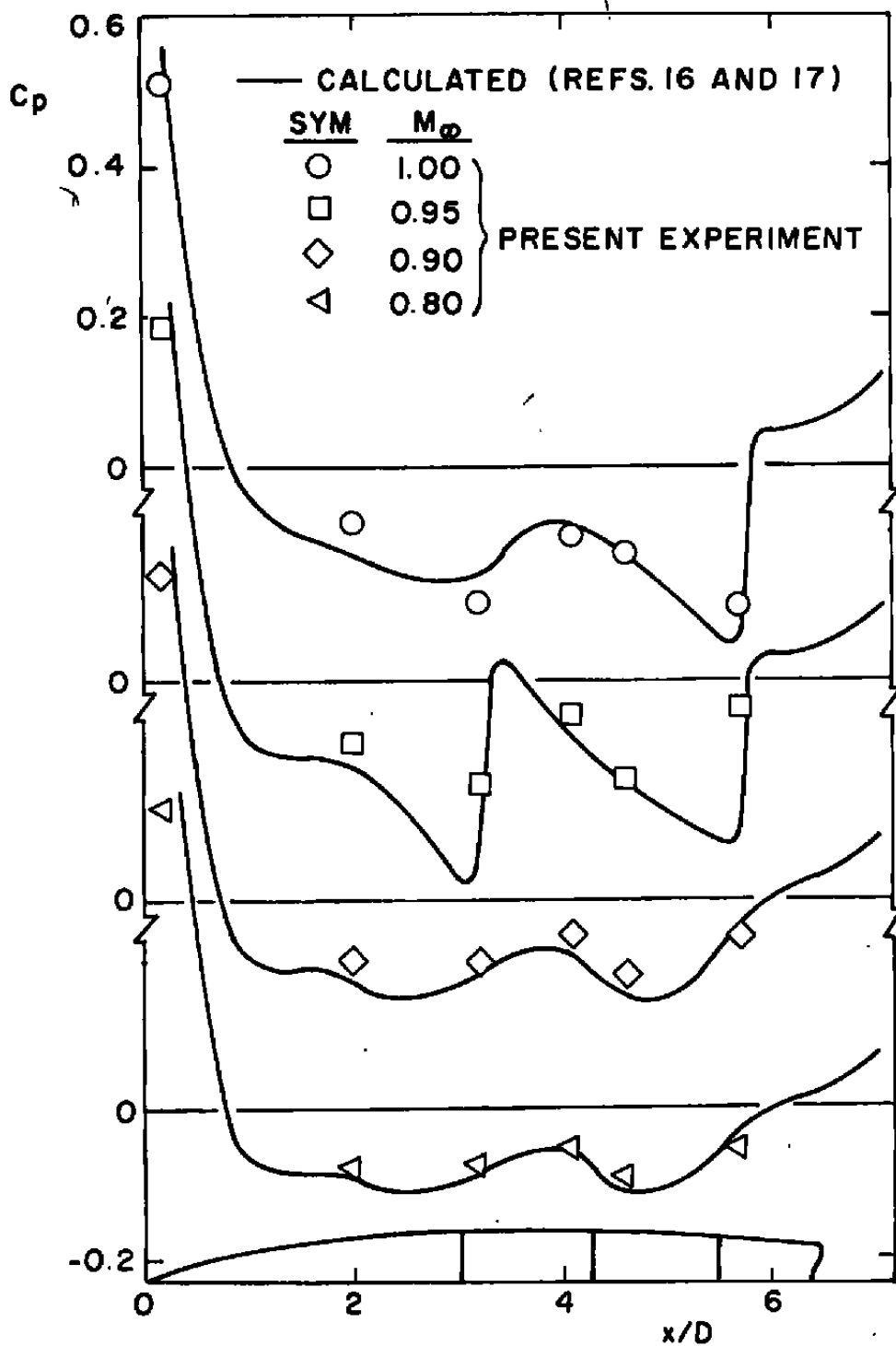
a. M_∞ = 0.8 through 1.0

Figure 20. Distribution of pressure on MK-83 store (configuration 011).

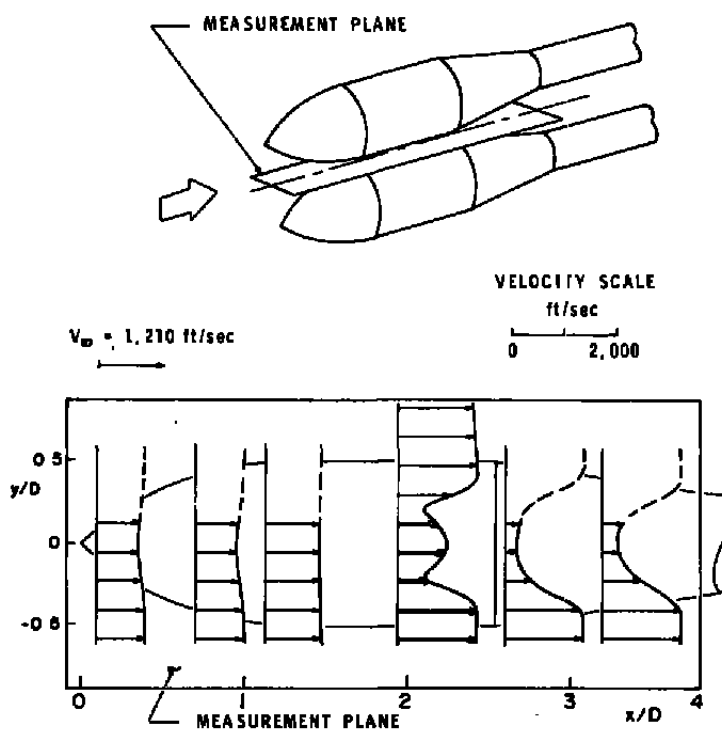46
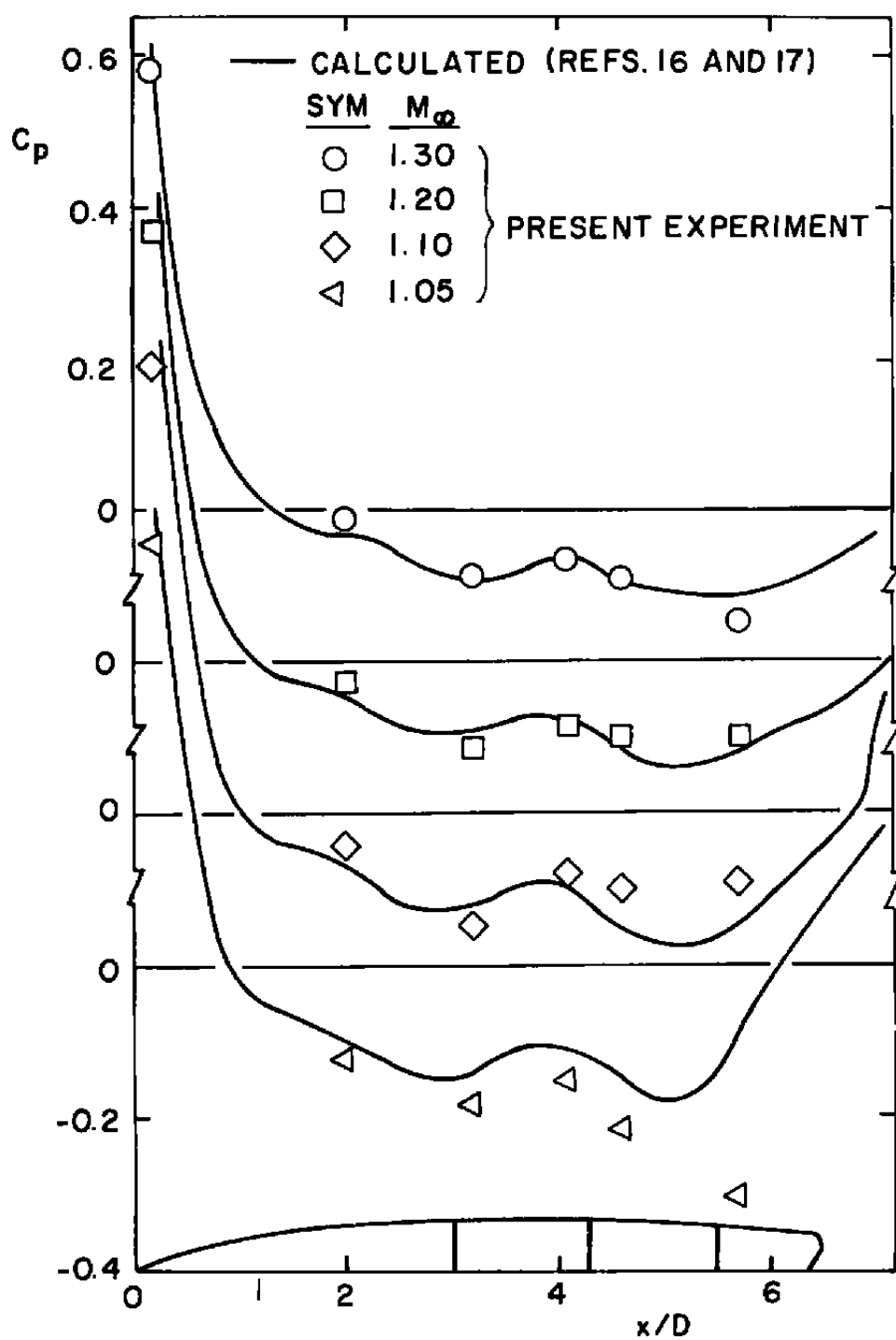
b. M_∞ = 1.05 through 1.30
Figure 20. Concluded.

MEASUREMENT PLANE

$V_\infty = 922$ ft/sec

VELOCITY SCALE
ft/sec

0   1,000

z/D

0.5

0

-0.5

-1.0

-1.5

0   2   4   6

x/D
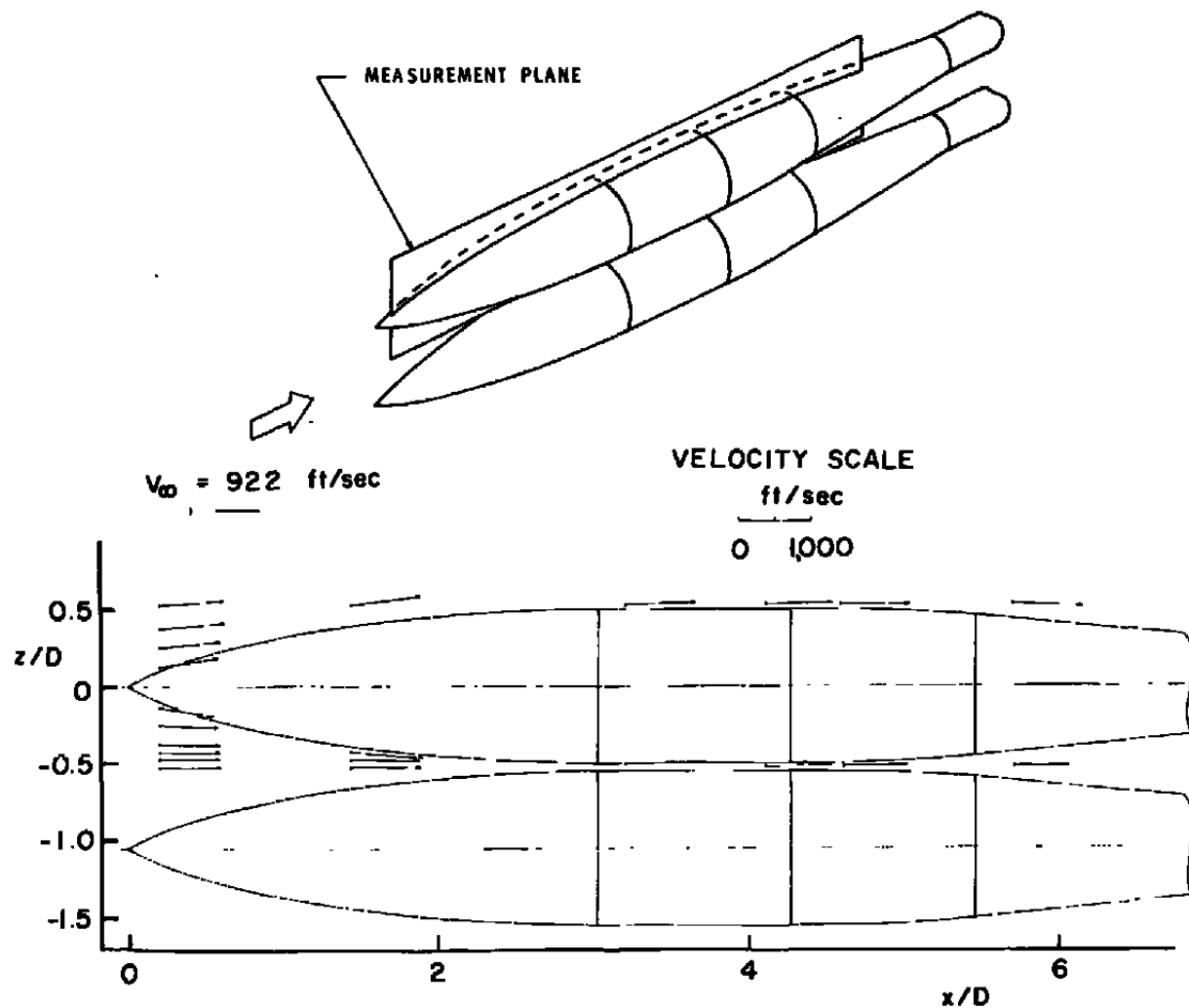
a. Configuration 012

Figure 21. Flow-field vector projections in constant y plane for
two-store configurations, $M_\infty = 0.80$, y/D = 0.

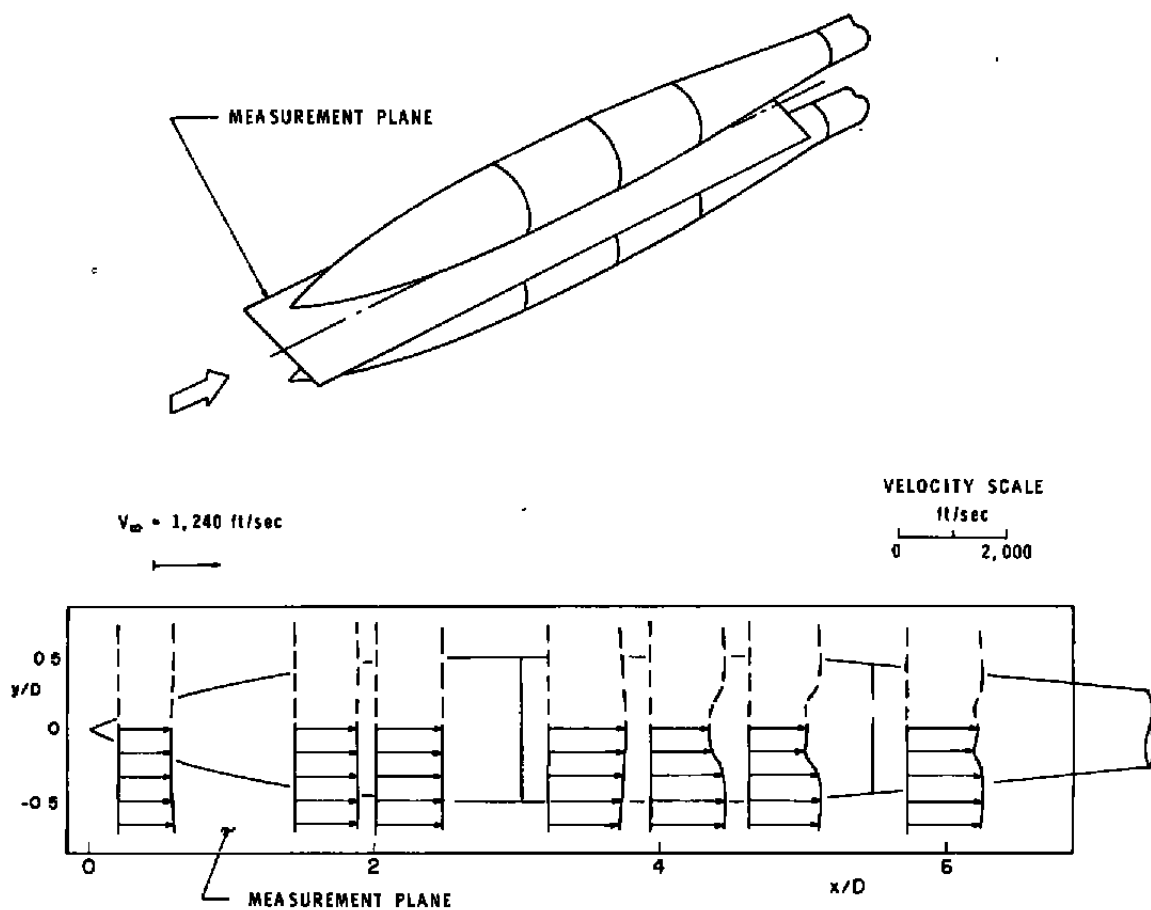MEASUREMENT PLANE

VELOCITY SCALE
ft/sec

V_∞ = 920 ft/sec

0   1,000

z/D

x/D
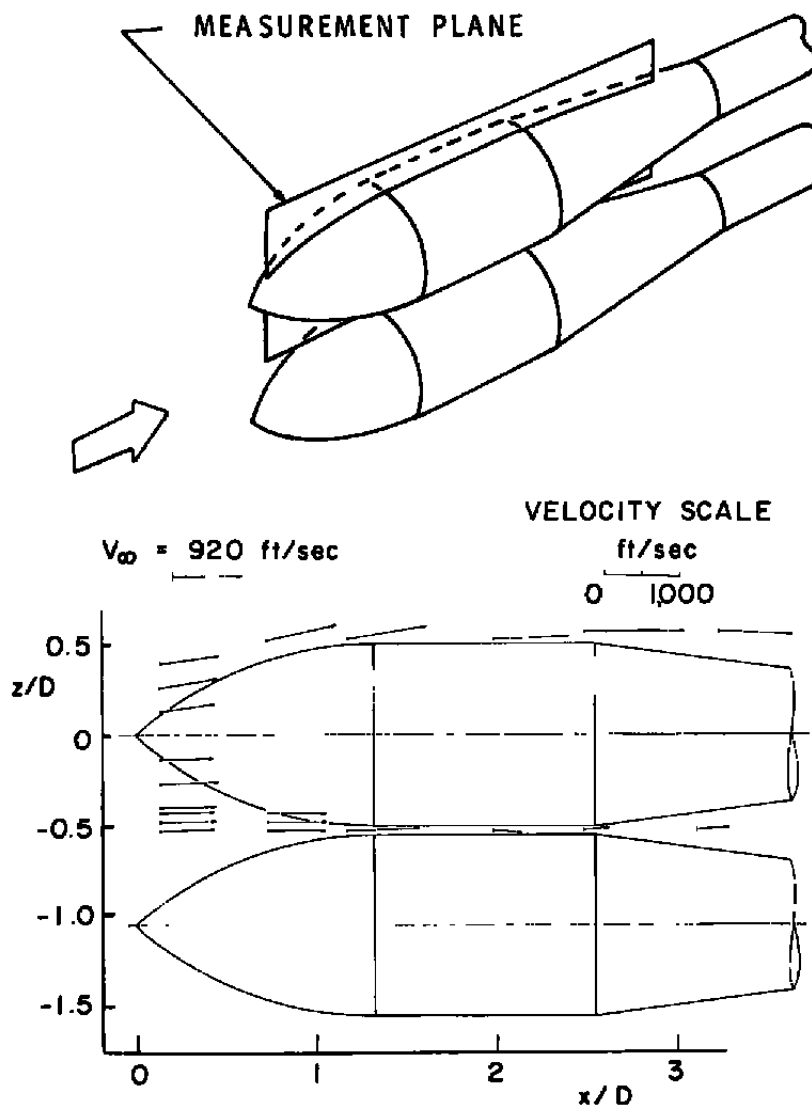
b. Configuration 022
Figure 21. Concluded.

a. Configuration 022

Figure 22. Axial velocity profiles in plane of symmetry between two stores, $M_\infty = 1.10$.

VELOCITY SCALE
ft/sec

V_∞ = 1,240 ft/sec

0   2,000

0 5
y/D

0

-0 5

0   2   4   6

x/D

MEASUREMENT PLANE

b. Configuration 012
Figure 22. Concluded.
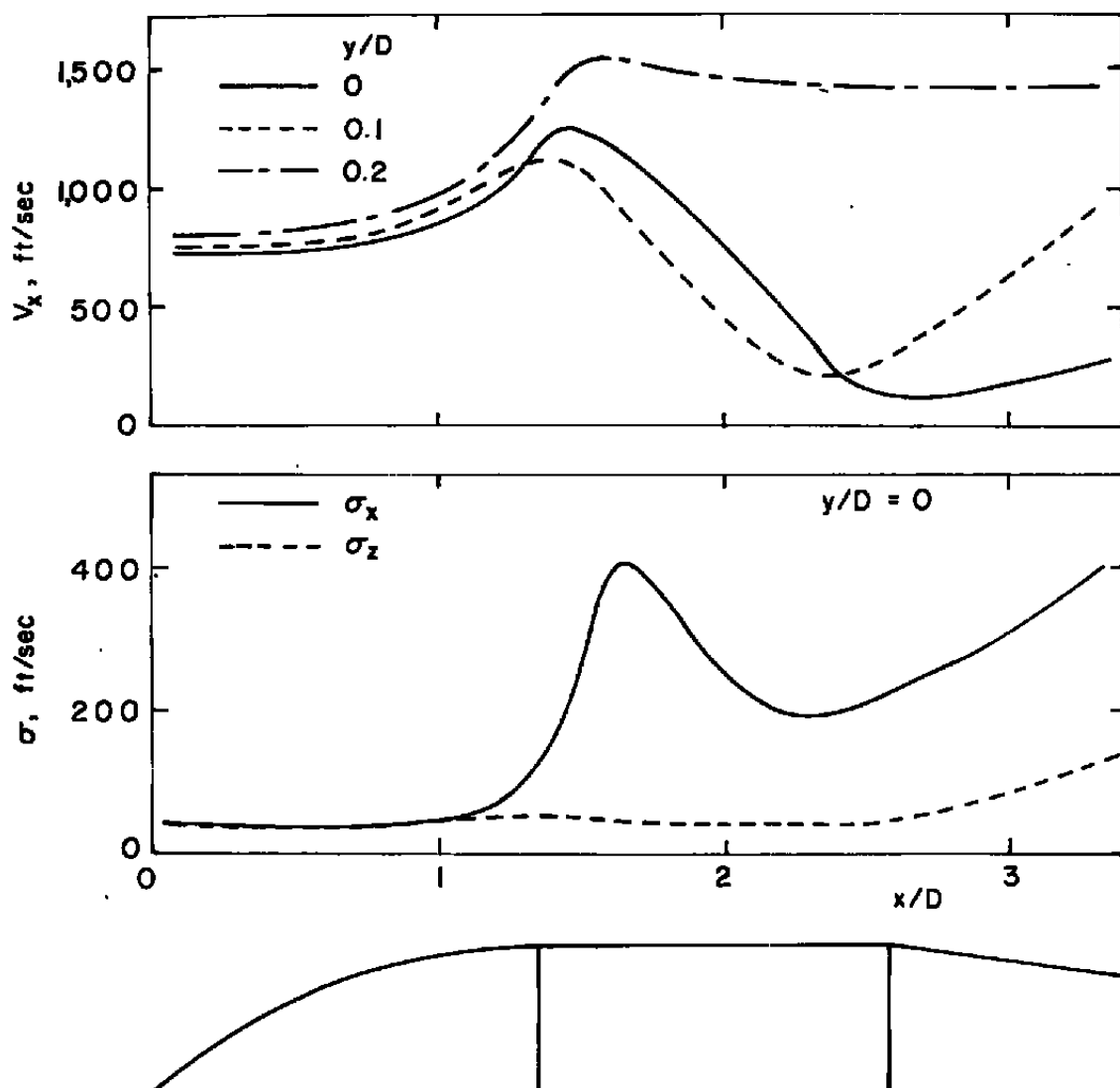
Figure 23. Mean and standard deviation of LV velocity measurements
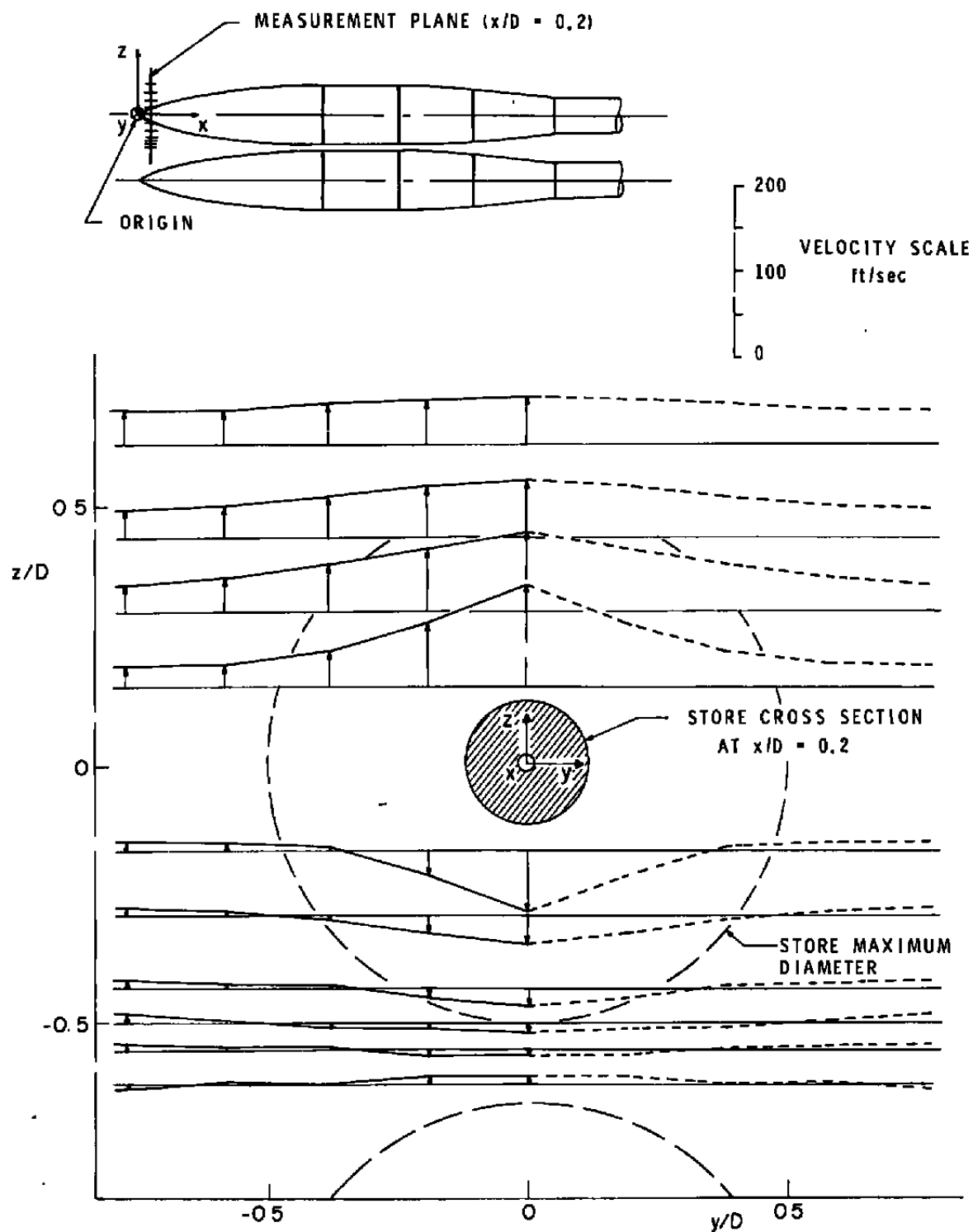in plane of symmetry between two M-117 stores
(configuration 022).

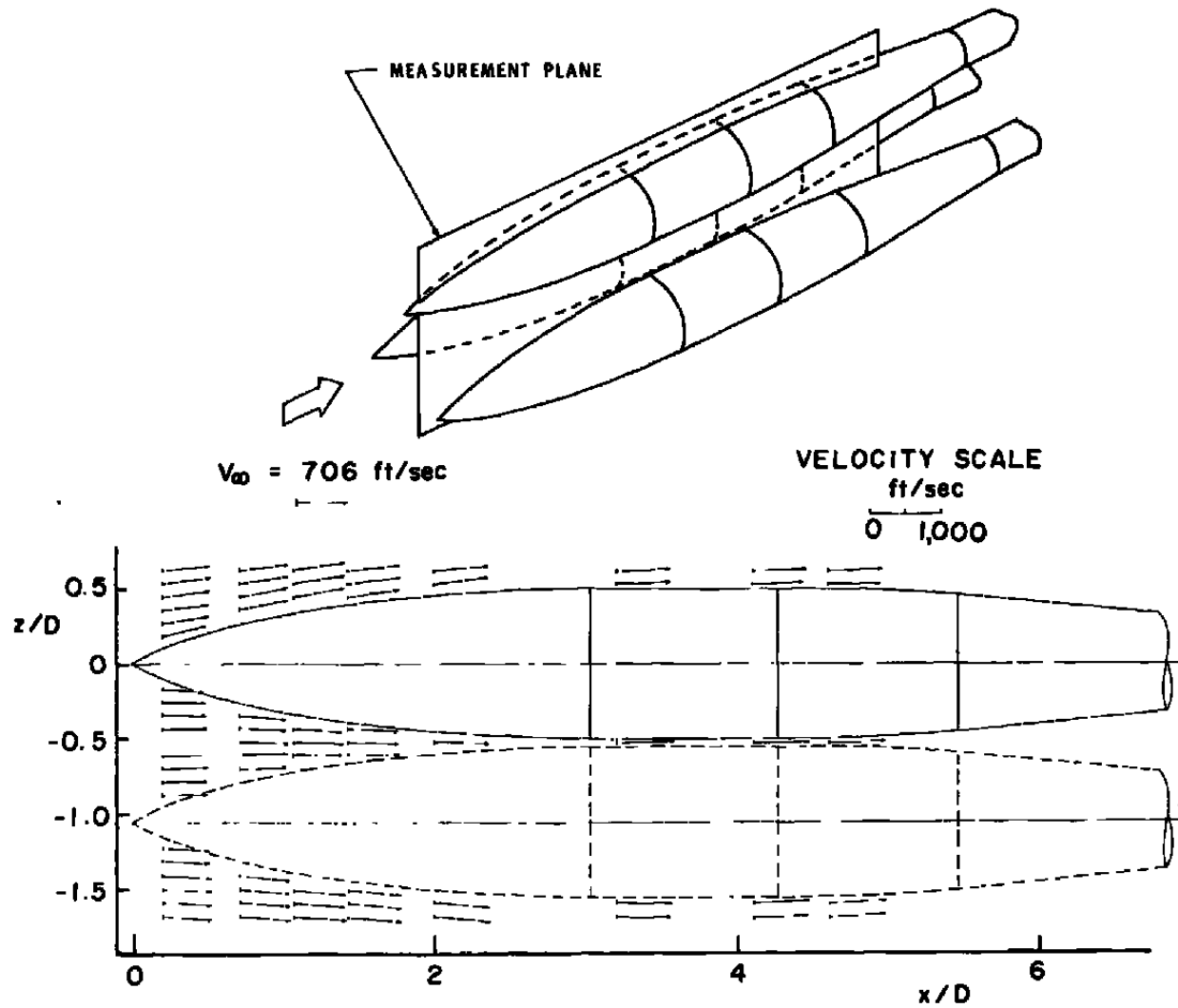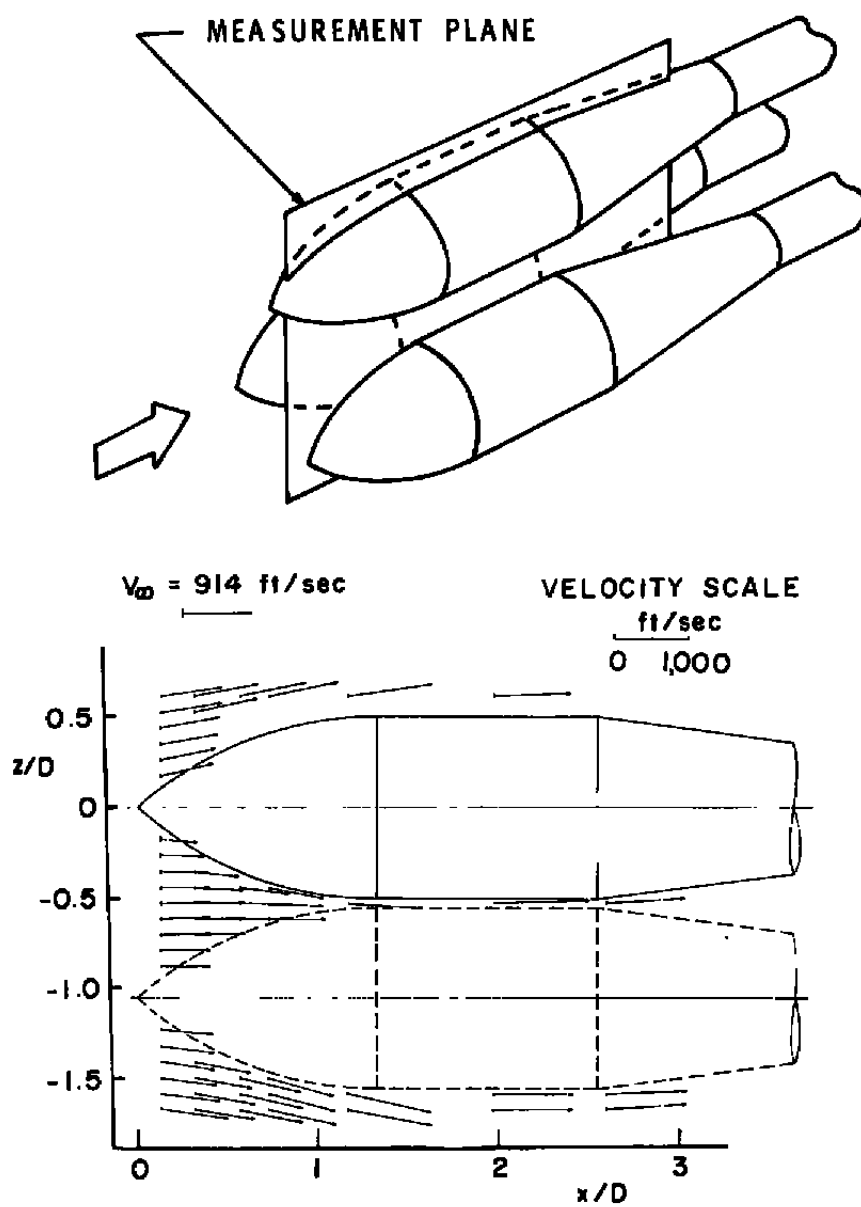Figure 24. V_y profiles in x/D = 0.2 plane (configuration 012), M_∞ = 0.80.

MEASUREMENT PLANE

V_∞ = 706 ft/sec

VELOCITY SCALE
ft/sec

0   1,000

z/D

0.5

0

-0.5

-1.0
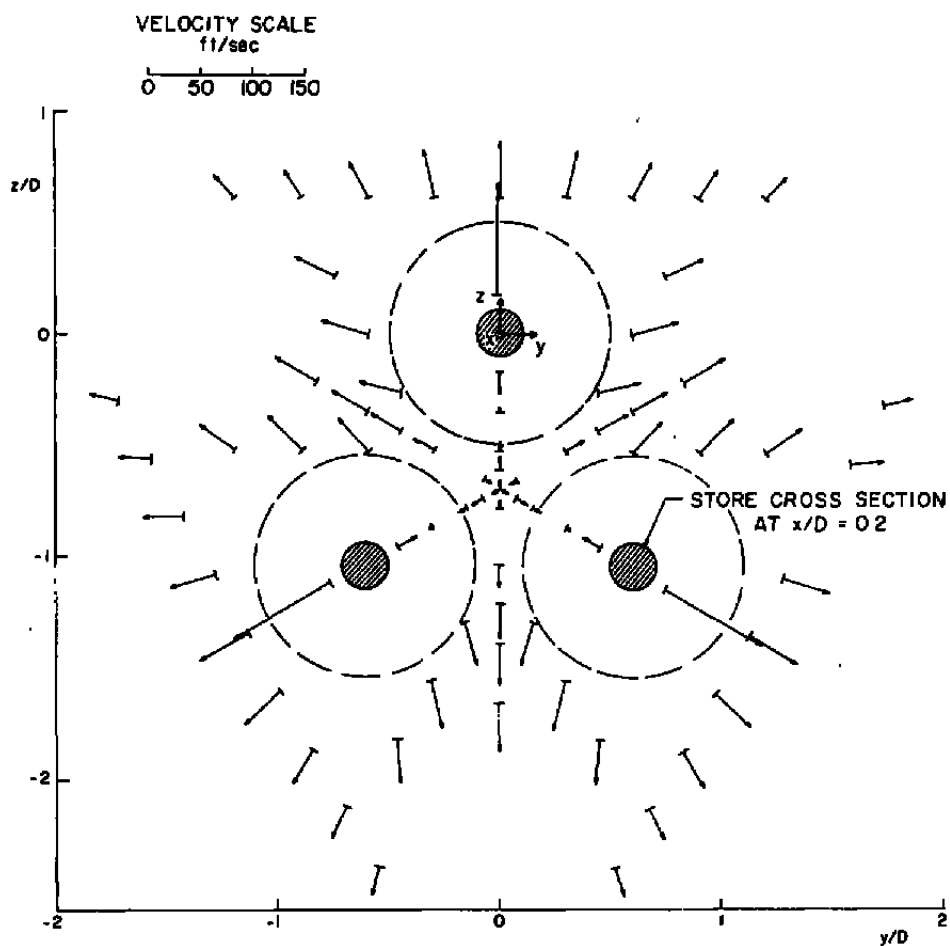
-1.5

0   2   4   6

x/D

a. Configuration 013, M_∞ = 0.60

Figure 25. Flow-field vector projections in constant y plane for
the three-store configurations, y/D = 0.

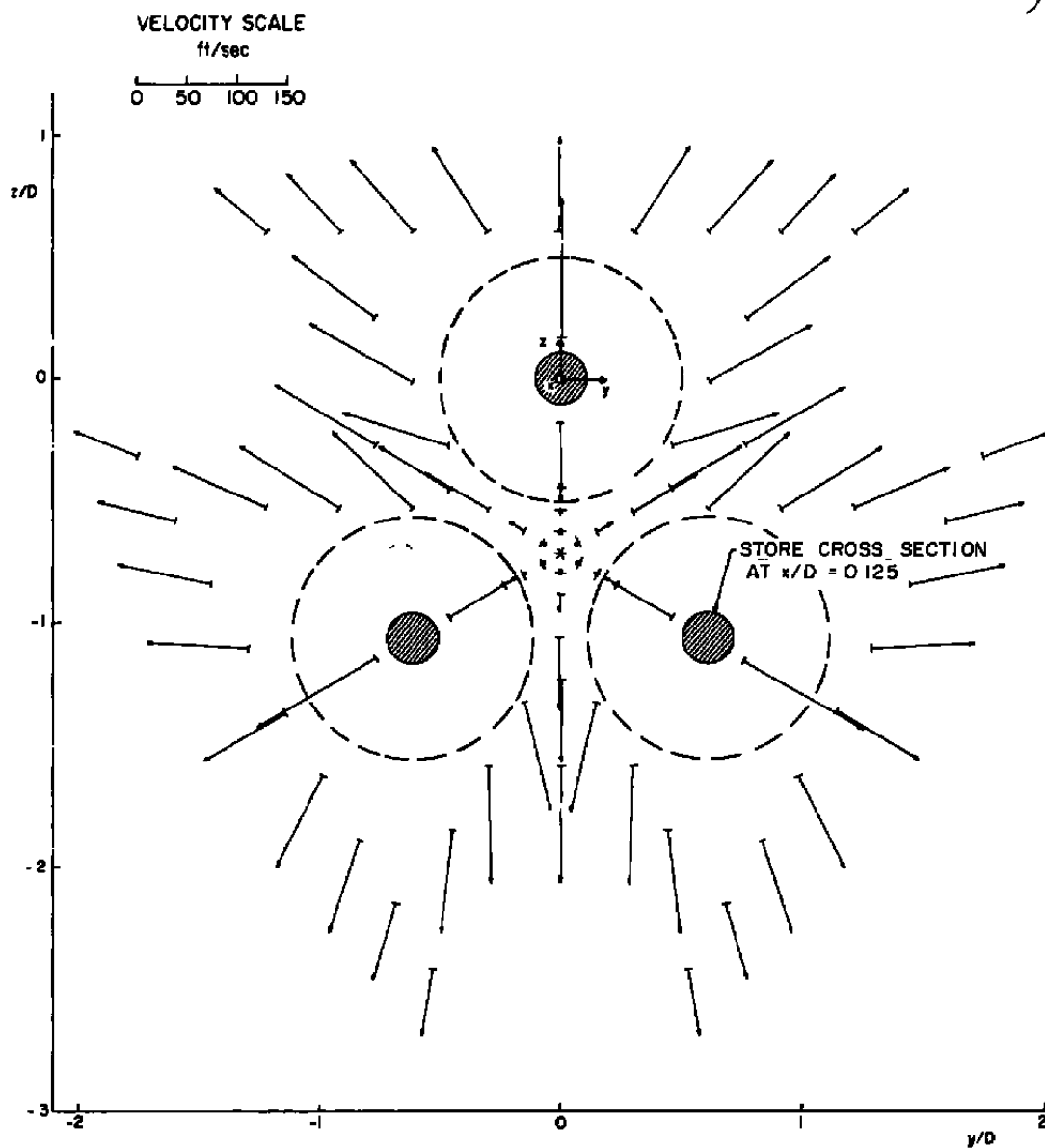b. Configuration 023, $M_\infty = 0.80$
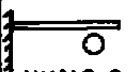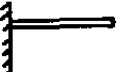Figure 25. Concluded.

a. Configuration 013
Figure 26. Resolved velocity vector projections in constant
z/D plane, M_∞ = 0.80.

b. Configuration 023
Figure 26. Concluded.

Table 1. Summary of Test Conditions

CONFIGURATION

MACH NUMBER	PHASE I		PHASE II			PHASE III	
	111	100	011	012	013	022	023
	WING & MK-83	WING	MK-83	MK-83	MK-83	M-117	M-117
0.60					● □		
0.80			●	● □	● □	● □ ▲	● □
0.85						● ▲	
0.87	● □ ◇ ▲						
0.90			●			● ▲	
0.92	● □ ◇ ▲	□ ◇	● □	● ▲			
0.95			●			● ▲	
1.00			● ▲			● ▲	
1.05			● ▲				
1.10			● ▲	● □ ▲		● □ ▲	
1.20			● ▲				
1.30			● □ ▲	● □ ▲		● □ ▲	

●   STORE SURFACE PRESSURES
◇   WING SURFACE PRESSURES
▲   SHADOWGRAPH
□   LASER VELOCIMETER FLOW-FIELD SURVEY

NOMENCLATURE

a	Axial distance from store nose, in. (Fig. 2)
c	Wing chord, in.
C_p	Local pressure coefficient, $(p - p_\infty)/q_\infty$
d	Local store diameter, in. (Fig. 2)
D	Store maximum diameter, in.
M_∞	Free-stream Mach number
M	Local Mach number
N	Number of stores (Fig. 4)
p	Local pressure measured at a model orifice, psfa
p_∞	Free-stream static pressure, psfa
q_∞	Free-stream dynamic pressure, psfa
S	Store identification number (Fig. 4)
t	Half-thickness of wing, in. (Fig. 2)
$V_x, V_y, V_z, V_{z'}$	Local velocity components obtained by the laser velocimeter, ft/sec
V_∞	Free-stream velocity from the standard tunnel system, ft/sec
W	Wing identification number (Fig. 4)
x,y,z	Cartesian coordinates, in. (Fig. 4)
x',y',z'	Cartesian coordinates rotated θ degrees about x axis, in. (Fig. 10)
x_w	Chordwise distance from wing leading edge, in. (Fig. 2)

σ   Standard deviation

θ   Angle of rotation of x′ y′ z′ coordinate system relative of xyz system about the x axis, deg (Fig. 10)

φ   Angle of a row of store pressure orifices relative to vertical, deg (Fig. 3)

SUBSCRIPTS

A,a,E,e,   Designated point in flow field (Fig. 10)

x,y,z   Indicate coordinate direction (Fig. 23)